THE UNIVERSITY OF ALABAMA
COLLEGE OF ENGINEERING
BUREAU OF ENGINEERING RESEARCH

(NASA-CR-144349) EVALUATION OF A COMPOSITE MOBILE HOLOGRAPHIC NONDESTRUCTIVE TEST SYSTEM Final Report (Alabama Univ., University.) 97 p HC $5.00 CSCL 14D
N76-26525
Unclas
G3/38 42337

FINAL REPORT

on

Contract NAS8-30479

# EVALUATION OF A COMPOSITE MOBILE HOLOGRAPHIC NONDESTRUCTIVE TEST SYSTEM

by

Hua-Kuang Liu
Principal Investigator

and

Ellis R. Commeens, William D. Hunt, and Larry Whitt
Research Assistants

Prepared for

National Aeronautics and Space Administration
George C. Marshall Space Flight Center
Marshall Space Flight Center, Alabama 35812

June 1976

BER Report No. 204-74



UA ... UNIVERSITY, ALABAMA

FINAL REPORT

on

Contract NAS8-30479

# EVALUATION OF A COMPOSITE MOBILE HOLOGRAPHIC NONDESTRUCTIVE TEST SYSTEM

by

Hua-Kuang Liu
Principal Investigator

and

Ellis R. Commeens, William D. Hunt, and Larry Whitt
Research Assistants

Prepared for

National Aeronautics and Space Administration
George C. Marshall Space Flight Center
Marshall Space Flight Center, Alabama 35812

June 1976

BER Report No. 204-74

# Preface

This final report describes work performed during the period June 1, 1975 to May 27, 1976 in fulfillment of the Contract No. NAS8-30479 entitled "An Evaluation of the Mobile HNDT System" funded by NASA MSFC. The research was conducted at the University of Alabama under the direction of Hua-Kuang Liu as Principal Investigator.

The Principal Investigator would like to acknowledge the continued encouragement and support by Dr. Robert L. Kurtz and Mr. Walding Moore of NASA, MSFC during the performance of the contract.

## Abstract

A simplified theoretical model for the interpretation of the double-exposure holographic interference fringe loci due to the general three-dimensional displacements has been derived for the specific composite mobile holographic non-destructive test (CMHNDT) system. The model, representing a good approximation to a more tedious theoretical result, predicts that a combination of in-plane and out-of-plane displacements of the surface will produce concentric circular-shaped fringe patterns with locations of their center affected by the displacements.

Appropriate experiments have been designed and carried out for the test of the validity of the theory. These experiments include the taking of double-exposure holograms of in-plane translations and combined in-plane and out-of-plane translations. Except for a few minor discrepancies, the simplified model agreed quite well with the experimental results.

In addition, experimentally observed effects due to the curvature of the test plate and the variations of the angles of incidence of the laser light suggest that in order for the simplified model to be able to predict the test results more accurately, incidence and reflection of the laser light should be chosen as nearly perpendicular to the surface of the tested object as possible. This point is especially important when the surface of the object is not flat.

Finally, the findings suggest that a calibration plate should be incorporated into the system for a more accurate quantitative assessment of the displacements on the surface of the object under test.

Table of Contents

## List of Figures

List of Figures (cont.)

List of Tables

## I. INTRODUCTION

Since the first proposal of the technique of wavefront reconstruction by Gabor[1] in 1947, holographic interferometry with the assistance of the laser[2] has come a long way both in theory and in its applications[3-18]. However, as it was discussed in a previous report[19], a quantitative evaluation of the interference fringes is difficult to perform practically. In addition, any quantitative analysis is usually system dependent, i.e., the analysis is dependent on the path length of the reference and object light beams, the angles between these beams and the normal direction of the object surface, the location of the point of observation, etc. Consequently, each system needs individual treatment with regard to the aspect of fringe evaluations.

The system studied in this contract is called a composite mobile holographic nondestructive test (CMHNDT) system invented by R. L. Kurtz[20]. The main approach of the study was to experimentally calibrate the optical CMHNDT system by a mechanical system which consists of ultra-accurate micrometers monitored by Michelson interferometers. A simplified, quantitative theoretical model based on the work of N. L. Hecht, et al[21], has been derived and the comparison of this model with the experimental results based on test samples with flat surfaces has been completed. Objects with curve surfaces of a variety of curvatures have also been used to determine qualitatively, the degree of the validity of the model in the case of a more general object under test.

Section II of the report will be a derivation of the theoretical model for the fringe interpretation. The experimental set-up and results are given in Sec. III. Discussions and a comparison of the simplified theory and the experiments will be contained in Sec. IV; and finally, Sec. V will provide the conclusions.

# II. THEORETICAL MODEL

## A. Derivation of the Model for Simple Translations

The CMHNDT system which this study investigates is illustrated by the block diagram shown in Fig. 1. The object in the diagram is mounted on an ultra-accurate micrometer-controlled translation stage with 2.54 μm/step movement. For the purpose of analyzing the interference fringes in the system, double exposure holograms are made with a displacement, described by the vector $\vec{D}$, of the object between the two exposures. The fringe contrast between any two points on the object is produced by the path length difference, $\delta\Delta L$, resulting from the object displacement at these two points. A more detailed description and a theoretical derivation of the model for the system is provided below.

In Fig. 2, it is assumed that the front surface of the object coincides with the x-y plane of the Cartesian coordinate system and $\hat{i}$, $\hat{j}$, and $\hat{k}$ are the unit vectors along the x-, y- and z-direction respectively. The vector $\vec{S}$ represents the distance from the laser source to the origin which is located on the test plate and $\vec{H}$, the distance from that origin to the observation point on the hologram. For the sake of simplicity, $\vec{S}$ and $\vec{H}$ are assumed to be co-planar with the x-z plane. The angles $\theta_S$ and $\theta_H$ are made by $\vec{S}$ and $\vec{H}$ with the x-axis respectively. Point 1' is displaced from its original position point 1 with a displacement vector $\vec{D}$. The vectors $\vec{t}$ and $\vec{R}$ are distances from the origin to point 1 and point 1' respectively. $\vec{S}_1$, $\vec{S}_2$, $\vec{H}_1$ and $\vec{H}_2$ are distances from the laser source to point 1 and point 1' and from these two points to the observation point at the hologram.

From the above description, the relationship among the vectors can be written as

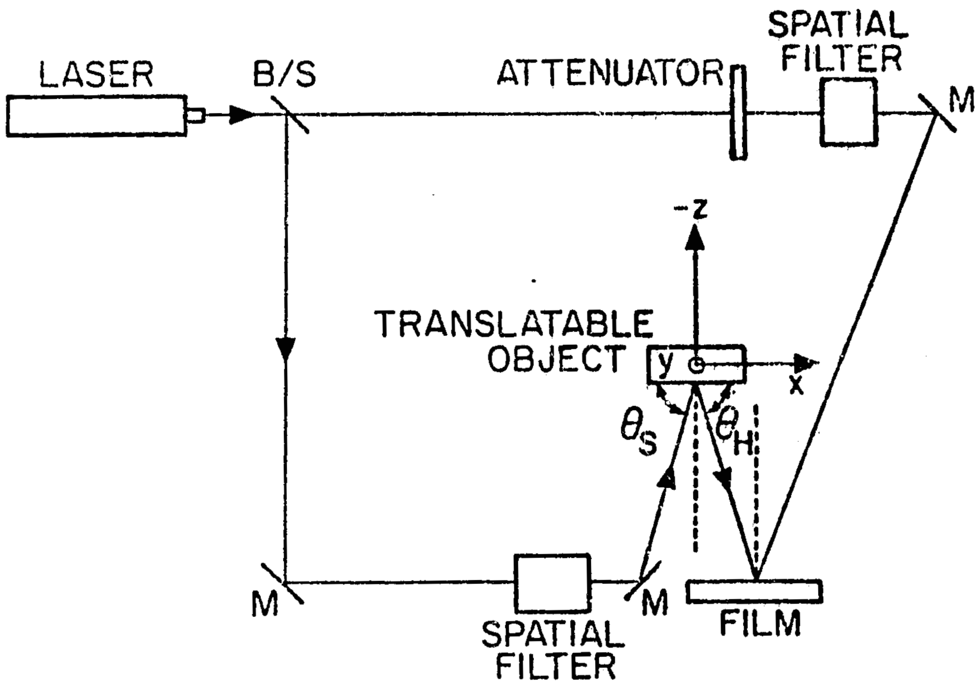


Figure 1. A Block Diagram of the CMHNDT System

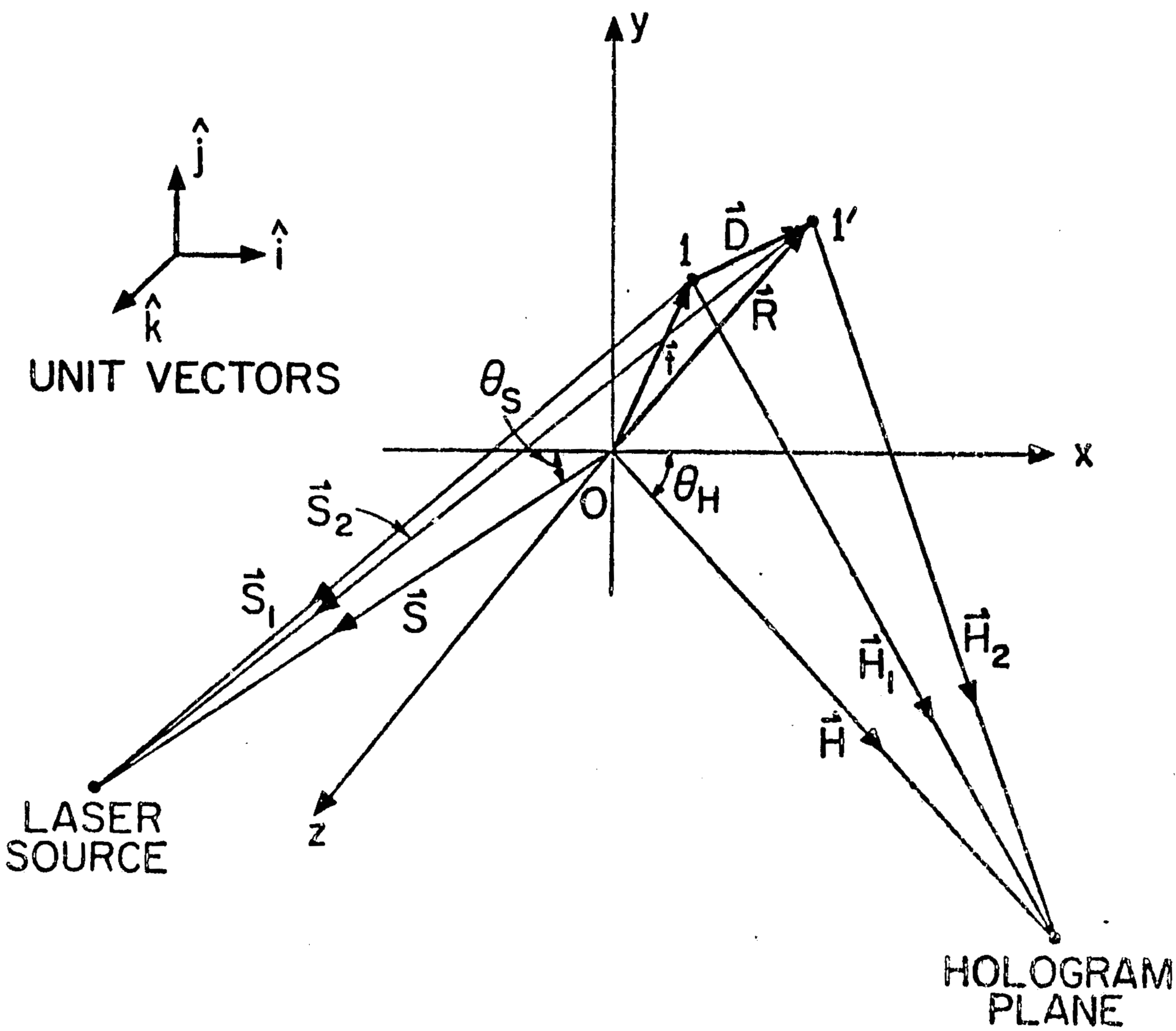


Figure 2. Vector diagram for the CMHNDT system with the front surface of the flat object coinciding with the x-y plane.

$$\vec{S} = \vec{S}_1 + \vec{t} = \vec{S}_2 + \vec{R} \ , \tag{1}$$

$$\vec{H} = \vec{H}_1 + \vec{t} = \vec{H}_2 + \vec{R} \ , \tag{2}$$

$$\vec{R} = \vec{D} + \vec{t} \ , \tag{3}$$

and

$$\vec{t} = x\hat{i} + y\hat{j} \ . \tag{4}$$

Furthermore, the normalized distances $\vec{S}/S$ and $\vec{H}/H$ may be written as

$$\vec{S}/S = -\cos\theta_S \ \hat{i} + \sin\theta_S \ \hat{k} \ , \tag{5}$$

and

$$\vec{H}/H = \cos\theta_H \ \hat{i} + \sin\theta_H \ \hat{k} \ . \tag{6}$$

With these notations, the path length difference $\Delta L$ of the light due to the displacement $\vec{D}$ from point 1 to point 1', may be defined as

$$\Delta L \equiv S_2 - S_1 + H_2 - H_1 \ . \tag{7}$$

From Eqs. (1) and (2), it can be shown that

$$\begin{aligned} S_1 &= (\vec{S}_1 \cdot \vec{S}_1)^{1/2} \\ &= [(\vec{S} - \vec{t}) \cdot (\vec{S} - \vec{t})]^{1/2} \\ &= [S^2 - 2(\vec{t} \cdot \vec{S}) + t^2]^{1/2} \\ &= S[1 - 2(\vec{t} \cdot \vec{S})/S^2 + t^2/S^2]^{1/2} \ , \end{aligned} \tag{8}$$

Similarly,

$$S_2 = [(\vec{S} - \vec{R}) \cdot (\vec{S} - \vec{R})]^{1/2}$$
$$= [S^2 - 2(\vec{R} \cdot \vec{S}) + R^2]^{1/2}$$
$$= [S^2 - 2(\vec{t} \cdot \vec{S}) - 2(\vec{D} \cdot \vec{S}) + t^2 + 2(\vec{t} \cdot D) + D^2]^{1/2} , \qquad (9)$$

where R was replaced by $\vec{D} + \vec{t}$ based on Eq. (3).

Generally, $|2(\vec{t} \cdot \vec{S})/S^2 - t^2/S^2| << 1$, (this condition is normally true or can be made valid for the system), then from the binomial expansion of Eq. (8), including up to the second order terms,

$$S_1 \simeq S\{1 - (1/2)[2(\vec{t} \cdot \vec{S})/S^2 - t^2/S^2]$$
$$- (1/8)[2(\vec{t} \cdot \vec{S})/S^2 - t^2/S^2]^2\} , \qquad (10)$$

or,

$$S_1 \simeq S - (\vec{t} \cdot \vec{S})/S + t^2/2S - (1/8S^3)[2(\vec{t} \cdot \vec{S}) - t^2]^2 . \qquad (11)$$

Similarly, under the condition $\left|\frac{2(\vec{t} \cdot \vec{S})}{S^2} + \frac{2(\vec{D} \cdot \vec{S})}{S^2} - \frac{t^2}{S^2} - \frac{D^2}{S^2} - \frac{2(\vec{t} \cdot \vec{D})}{S^2}\right| << 1$,

$$S_2 \simeq S\{1 - (1/2)[\frac{2(t \cdot S)}{S^2} + \frac{2(D \cdot S)}{S^2} - \frac{t^2}{S^2} - \frac{D^2}{S^2} - \frac{2(t \cdot D)}{S^2}]$$
$$- (1/8)[\frac{2(t \cdot S)}{S^2} + \frac{2(D \cdot S)}{S^2} - \frac{t^2}{S^2} - \frac{D^2}{S^2} - \frac{2(t \cdot D)}{S^2}]^2\} . \qquad (12)$$

From Eqs. (11) and (12),

$$S_2 - S_1 \simeq \frac{\vec{t} \cdot \vec{D}}{S} + \frac{D^2}{2S} - \frac{\vec{D} \cdot \vec{S}}{S}$$
$$+ \frac{1}{8S^3} \{[2(\vec{t} \cdot \vec{S}) - t^2]^2 - [2(\vec{t} \cdot \vec{S}) + 2(\vec{D} \cdot \vec{S})$$
$$- t^2 - D^2 - 2(\vec{t} \cdot \vec{D})]^2\} ,$$

or

$$S_2 - S_1 = \{\frac{\vec{t} \cdot \vec{D}}{S} + \frac{D^2}{2S} - \frac{\vec{D} \cdot \vec{S}}{S}\}$$

$$+ \{\frac{1}{8S^3} [4(\vec{t} \cdot \vec{S}) + 2(\vec{D} \cdot \vec{S}) - 2t^2 - D^2 - 2(\vec{t} \cdot \vec{D})]x$$

$$[-2(\vec{D} \cdot \vec{S}) + D^2 + 2(\vec{t} \cdot \vec{D}]\} , \qquad (13)$$

where the first { } in Eq. (13) contains the first order terms and the second { } contains the second order terms in the approximation.

Analogous to the above approach and from Eqs. (2) and (3),

$$H_1^2 = H^2 - 2(\vec{t} \cdot \vec{H}) + t^2 ,$$

$$H_2^2 = H^2 - 2(\vec{t} \cdot \vec{H}) - 2(\vec{D} \cdot \vec{H}) + t^2$$

$$+ 2(\vec{t} \cdot \vec{D}) + D^2 .$$

The difference $H_2 - H_1$, including the second order approximation, may be written as

$$H_2 - H_1 \simeq \{\frac{\vec{t} \cdot \vec{D}}{H} + \frac{D^2}{2H} - \frac{\vec{D} \cdot \vec{H}}{H}\}$$

$$+ \{\frac{1}{8H^3} [4(\vec{t} \cdot \vec{H}) + 2(\vec{D} \cdot \vec{H}) - 2t^2 - D^2 - 2(\vec{t} \cdot \vec{D})]x$$

$$[-2(\vec{D} \cdot \vec{H}) + D^2 + 2(\vec{t} \cdot \vec{D})]\} . \qquad (14)$$

The total optical path length difference $\Delta L$ between 1 and 1' with second order approximation can be written as

$$\Delta L = S_2 - S_1 + H_2 - H_1$$

$$\simeq \{(\frac{1}{S} + \frac{1}{H})(\vec{t}\cdot\vec{D} + \frac{D^2}{2}) - \vec{D} \cdot (\frac{\vec{S}}{S} + \frac{\vec{H}}{H})\}$$

$$+ \frac{1}{2}\{\frac{1}{S^3}[2(\vec{t}\cdot\vec{S}) + (\vec{D}\cdot\vec{S}) - (\vec{D}\cdot\vec{t}) - t^2 - \frac{D^2}{2}] \times [-(\vec{D}\cdot\vec{S}) + (\vec{D}\cdot\vec{t}) + \frac{D^2}{2}]$$

$$+ \frac{1}{H^3}[2(\vec{t}\cdot\vec{H}) + (\vec{D}\cdot\vec{H}) - (\vec{D}\cdot\vec{t}) - t^2 - \frac{D^2}{2}] \times [(-\vec{D}\cdot\vec{H}) + (\vec{D}\cdot\vec{t}) + \frac{D^2}{2}]\} , \quad (15)$$

It is convenient to define the first order term in Eq. (15) as $(\Delta L)_1$ and the second order term as $(\Delta L)_2$ and write

$$\Delta L \simeq (\Delta L)_1 + (\Delta L)_2 , \quad (16)$$

where

$$(\Delta L)_1 \equiv (\frac{1}{S} + \frac{1}{H})(\vec{t} \cdot \vec{D} + \frac{D^2}{2}) - \vec{D} \cdot (\frac{\vec{S}}{S} + \frac{\vec{H}}{H}) , \quad (17)$$

and

$$(\Delta L)_2 \equiv \frac{-1}{2S^3}[2(\vec{t}\cdot\vec{S}) + (\vec{D}\cdot\vec{S}) - (\vec{D}\cdot\vec{t}) - t^2 - \frac{D^2}{2}] \times [(\vec{D}\cdot\vec{S}) - (\vec{D}\cdot\vec{t}) - \frac{D^2}{2}]$$

$$- \frac{1}{2H^3}[2(\vec{t}\cdot\vec{H}) + (\vec{D}\cdot\vec{H}) - (\vec{D}\cdot\vec{t}) - t^2 - \frac{D^2}{2}] \times [(\vec{D}\cdot\vec{H}) - (\vec{D}\cdot\vec{t}) - \frac{D^2}{2}] . \quad (18)$$

When $\vec{D} = D_x \hat{i} + D_y \hat{j} + D_z \hat{k}$ is substituted into Eq. (17),

$$(\Delta L)_1 = (\frac{1}{S} + \frac{1}{H})[D_x x + D_y y + \frac{1}{2}(D_x{}^2 + D_y{}^2 + D_z{}^2)]$$

$$- [(\cos\theta_H - \cos\theta_S) D_x + (\sin\theta_H + \sin\theta_S) D_z] . \quad (19)$$

The fringe contrast due to the displacement $\vec{D}$ between point 1 and the origin as one views through the double-exposure hologram is caused by the difference between the path length differences (or phase differences), $\delta(\Delta L)$, at point 1 and at the origin. The mathematical expression $\delta(\Delta L_1)$, where the subscript 1 denotes the first order term, may be defined as

$$\delta(\Delta L_1) \equiv (\Delta L_1)_{\text{at }(x,y)} - (\Delta L_1)_{\text{at }(0,0)} \; . \tag{20}$$

Applying Eq. (19), one finds

$$\begin{aligned}\delta(\Delta L_1) &= (\frac{1}{S} + \frac{1}{H})\, D_x x + (\frac{1}{S} + \frac{1}{H})\, D_y y \\ &= Ax + By \end{aligned} \tag{21}$$

where

$$A \equiv (\frac{1}{S} + \frac{1}{H})\, D_x \; , \tag{22}$$

and

$$B \equiv (\frac{1}{S} + \frac{1}{H})\, D_y \; . \tag{23}$$

At the moment, if all the higher order terms are neglected, one may relate $\delta(\Delta L_1)$ to the fringes as follows

$$\begin{aligned}\delta(\Delta L_1) &= Ax + By \\ &= (2n - 1)\lambda/2 \; , \end{aligned} \tag{24}$$

where $n$ is an ordinal number indicating the fringe order at (x,y) with respect to the origin, and $\lambda$ is the wavelength of the laser.

The physical meaning of Eq. (24) may be classified by the following three points:

(1) If $D_x = 0$, the fringes on the surface of the object are parallel to the x-axis with a separation of $\lambda/2B$ between any two neighboring fringes; if $D_y = 0$, the fringes are perpendicular to the x-axis with a separation of $\lambda/2A$ between any two neighboring fringes. If both $D_x$ and $D_y$ are not zero, then slanting fringes will appear.

(2) $\lambda/2A$ decreases as $D_x$ increases and $\lambda/2B$ decreases as $D_y$ increases, therefore the fringe spacing is denser when the magnitude of the displacement is larger.

(3) The first order approximation is not capable of predicting the effect of $D_z \neq 0$. Therefore, the theory is only good for the case that $D_z = 0$.

Points (1) and (2) above can better be illustrated by Fig. 3(a) and (b).

In order to see the effect of $D_z \neq 0$, it is necessary to consider the second order terms. Following the definition given by Eq. (20) and from Eq. (18), it can be shown (see Appendix A) that

$$
\begin{aligned}
\delta(\Delta L_2) = & -\frac{1}{2}\left(\frac{1}{S^3}+\frac{1}{H^3}\right)(\vec{D}\cdot\vec{t})t^2 \\
& + \left\{\frac{1}{2}\left[\vec{D}\cdot\left(\frac{\vec{S}}{S^3}+\frac{\vec{H}}{H^3}\right) - \frac{1}{2}\left(\frac{1}{S^3}+\frac{1}{H^3}\right)D^2\right]t^2\right. \\
& \left. - \frac{1}{2}\left(\frac{1}{S^3}+\frac{1}{H^3}\right)(\vec{D}\cdot\vec{t})^2 + \left[\left(\frac{\vec{S}}{S^3}+\frac{\vec{H}}{H^3}\right)\cdot\vec{t}\right](\vec{D}\cdot\vec{t})\right\} \\
& - \left\{\left[\left(\frac{1}{S^3}+\frac{1}{H^3}\right)\frac{D^2}{2} - \vec{D}\cdot\left(\frac{\vec{S}}{S^3}+\frac{\vec{H}}{H^3}\right)\right](\vec{D}\cdot\vec{t}) - \frac{D^2}{2}\left(\frac{\vec{S}}{S^3}+\frac{\vec{H}}{H^3}\right)\cdot\vec{t}\right. \\
& \left. + \frac{1}{S^3}(\vec{S}\cdot\vec{D})(\vec{S}\cdot\vec{t}) + \frac{1}{H^3}(\vec{H}\cdot\vec{D})(\vec{H}\cdot\vec{t})\right\}
\end{aligned} \tag{25}
$$

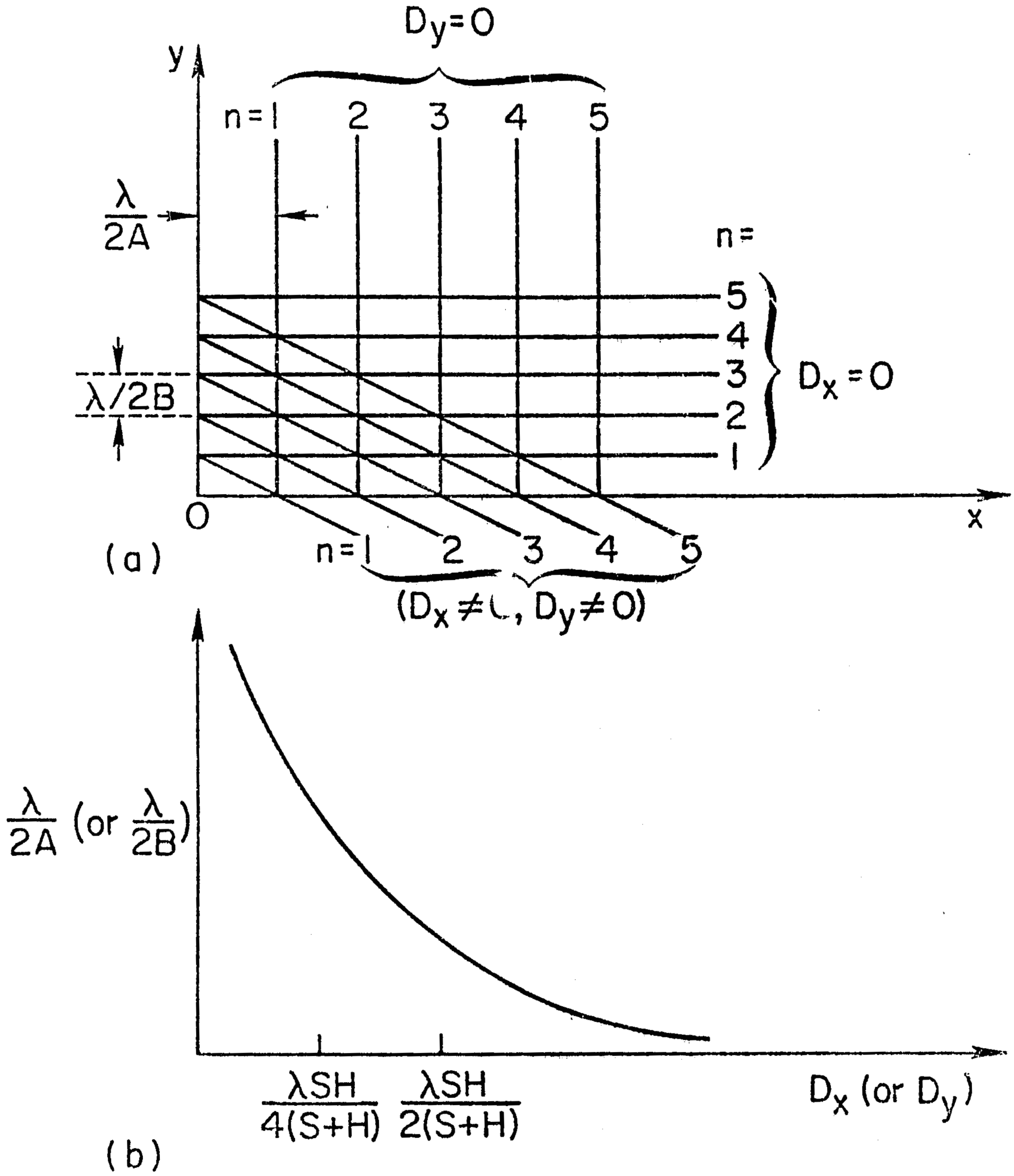


Figure 3. Relationship between displacements $D_x$ and $D_y$ and fringe location (x,y) with only the first order approximation, (a) cases for ($D_x$=0, $D_y\neq$0), ($D_x\neq$0,$D_y$=0), and ($D_x\neq$0,$D_y\neq$0); (b) $\lambda$/2A (or $\lambda$/2B) versus $D_x$ (or $D_y$).

when $D = D_x\hat{i} + D_y\hat{j} + D_z\hat{k}$ and $t = x\,\hat{i} + y\,\hat{j}$ are substituted into Eq. (25), which represents the second order part of the difference of the path length differences. After this result is combined with the first order terms given by Eq. (21), the fringe loci, including second order approximation, are obtained as follows:

$$\delta(\Delta L_{1,2}) \equiv \delta(\Delta L_1) + \delta(\Delta L_2)$$

$$= -\frac{1}{2}\left(\frac{1}{S^3} + \frac{1}{H^3}\right)(D_x x + D_y y)(x^2 + y^2)$$

$$+ \left\{\frac{1}{2}\left[D_x\left(\frac{-\cos\theta_S}{S^2} + \frac{\cos\theta_H}{H^2}\right) + D_z\left(\frac{\sin\theta_S}{S^2} + \frac{\sin\theta_H}{H^2}\right)\right.\right.$$

$$\left. - \frac{1}{2}\left(\frac{1}{S^3} + \frac{1}{H^3}\right)(D_x^{\ 2} + D_y^{\ 2} + D_z^{\ 2})\right](x^2 + y^2)$$

$$- \frac{1}{2}\left(\frac{1}{S^3} + \frac{1}{H^3}\right)(D_x x + D_y y)^2$$

$$\left. + x\left(\frac{-\cos\theta_S}{S^2} + \frac{\cos\theta_H}{H^2}\right)(D_x x + D_y y)\right\}$$

$$- \left\{\left[\frac{1}{2}(D_x^{\ 2} + D_y^{\ 2} + D_z^{\ 2})\left(\frac{1}{S^3} + \frac{1}{H^3}\right) - D_x\left(\frac{-\cos\theta_S}{S^2} + \frac{\cos\theta_H}{H^2}\right)\right](D_x x + D_y y)\right.$$

$$\left. - \frac{1}{2}(D_x^{\ 2} + D_y^{\ 2} + D_z^{\ 2})\left(\frac{-\cos\theta_S}{S^2} + \frac{\cos\theta_H}{H^2}\right)x\right\}$$

$$+ \frac{1}{S}\left[-\cos\theta_S D_x + \sin\theta_S D_z\right]\cos\theta_S\, x$$

$$- \frac{1}{H}\left[\cos\theta_H D_x + \sin\theta_H D_z\right]\cos\theta_H\, x + \left(\frac{1}{S} + \frac{1}{H}\right)(D_x x + D_y y)$$

$$= \left(n - \frac{1}{2}\right)\lambda\ . \tag{26}$$

Equation (26) is a general expression for the effect up to a second order approximation of the translation-type displacement $\vec{D} = \vec{D}_x \hat{i} + \vec{D}_y \hat{j} + \vec{D}_z \hat{k}$ on the fringes in the CMHNDT system. The expression looks quite complicated, therefore, its physical meaning is not obvious without further manipulations. The approach, which will be adopted, is to first simplify the expression by defining some new symbols and then consider the possible special cases that may be tested by the experiments. One may let

$$P_1 \equiv \frac{1}{S^3} + \frac{1}{H^3} , \tag{27}$$

$$P_2 \equiv \frac{-\cos\theta_S}{S^2} + \frac{\cos\theta_H}{H^2} , \tag{28}$$

$$P_3 \equiv \frac{\sin\theta_S}{S^2} + \frac{\sin\theta_H}{H^2} , \tag{29}$$

$$P_4 \equiv \frac{\cos^2\theta_S}{S} + \frac{\cos^2\theta_H}{H} , \tag{30}$$

$$P_5 \equiv \frac{\sin\theta_S \cos\theta_S}{S} - \frac{\sin\theta_H \cos\theta_H}{H} . \tag{31}$$

Substituting Eqs. (27)-(31) into Eq. (26), one obtains

$$\begin{aligned}
\delta(\Delta L_{1,2}) \simeq & -\frac{1}{2} P_1 (D_x x + D_y y)(x^2 + y^2) \\
& + \frac{1}{2} [P_2 D_x + P_3 D_z - \frac{1}{2} P_1 D^2](x^2 + y^2) \\
& - \frac{1}{2} P_1 (D_x x + D_y y)^2 - P_2 (D_x x + D_y y) x \\
& - [\frac{1}{2} P_1 D^2 - P_2 D_x - (\frac{1}{S} + \frac{1}{H})](D_x x + D_y y) \\
& + \frac{1}{2} D^2 P_2 x - P_4 D_x x + P_5 D_z x = (n - \frac{1}{2}) \lambda .
\end{aligned} \tag{32}$$

The three special cases that can be tested by experiment are (i) $D_x = D_y = 0$, $D_z \neq 0$; (ii) $D_y = 0$, $D_x \neq 0$, and $D_z \neq 0$; and (iii) $D_x = 0$, $D_y \neq 0$, and $D_z \neq 0$. These cases are discussed separately below and appropriate approximations will be made later before the theory is compared to the experiment.

Case (i). When $D_x = D_y = 0$, $D_z \neq 0$ is substituted into Eq. (32),

$$\delta(\Delta L_{1,2}) = \frac{1}{2}\,(P_3 D_z - \frac{1}{2}\,P_1 D_z^{\,2})(x^2 + y^2) + (\frac{1}{2}\,D_z^{\,2} P_2 + P_5 D_z)x = (n - \frac{1}{2})\,\lambda \;. \tag{33}$$

Or alternatively, Eq. (33) may be written as

$$A_1\,(x^2 + y^2) + B_1 x = (n - \frac{1}{2})\,\lambda \;, \tag{34}$$

where

$$A_1 = \frac{1}{2}\,D_z\,(\frac{\sin\theta_S}{S^2} + \frac{\sin\theta_H}{H^2}) - \frac{1}{2}\,D_z^{\,2}\,(\frac{1}{S^3} + \frac{1}{H^3}) \;, \tag{35}$$

$$B_1 = \frac{D_z^{\,2}}{2}\,(\frac{-\cos\theta_S}{S^2} + \frac{\cos\theta_H}{H^2}) + D_z\,(\frac{\sin\theta_S\cos\theta_S}{S} - \frac{\sin\theta_H\cos\theta_H}{H}) \;. \tag{36}$$

Equation (34) signifies that the loci of the circular fringes are centered at $(-\frac{B_1}{2A_1}\,,\,0)$ with the $n^{th}$ radius having a value

$$R_n = \sqrt{\frac{B_1^{\,2}}{4A_1^{\,2}} + \frac{(n - \frac{1}{2})\,\lambda}{A_1}} \;. \tag{37}$$

Furthermore, if $\theta_S = \theta_H = \theta$, then Eqs. (35) and (36) become

$$A_1 = \frac{1}{2} D_z \left(\frac{1}{S^2} + \frac{1}{H^2}\right) \sin\theta - \frac{1}{2} D_z^{\ 2} \left(\frac{1}{S^3} + \frac{1}{H^3}\right) , \tag{38}$$

$$B_1 = \frac{1}{2} D_z^{\ 2} \left(\frac{-1}{S^2} + \frac{1}{H^2}\right) \cos\theta . \tag{39}$$

In addition, if one lets $S = H = T$, Eqs. (38) and (39) become

$$A_1 = \frac{D_z \sin\theta}{T^2} - \frac{D_z^{\ 2}}{T^3} \tag{40}$$

$$B_1 = 0 \tag{41}$$

and the fringe circles have their center at (0,0) with radii

$$R_n = (n - 1/2)\, \lambda / A_1 . \tag{42}$$

The result shown in Eq. (42) indicates that when $n$ is large, the radii proportionally approach those of a Fresnel zone plate. In general, the loci of the fringes for $D_z \neq 0$ and $D_x = D_y = 0$ can be illustrated by Fig. 4 with $A_1$ and $B_1$ given either by the pair Eqs. (35) and (36), Eqs. (38) and (39), or Eqs. (40) and (41) depending on the conditions under which each case occurs.

<u>Case (ii)</u>. When $D_x \neq 0$, $D_y = 0$, and $D_z \neq 0$ are substituted into Eq. (32), it becomes

$$\begin{aligned} &- \frac{1}{2} P_1 D_x (x^3 + xy^2) + \frac{1}{2} [P_2 D_x + P_3 D_z - \frac{1}{2} P_1 (D_x^{\ 2} + D_z^{\ 2})](x^2 + y^2) \\ &- \frac{1}{2} P_1 D_x^{\ 2} x^2 - P_2 D_x x^2 - [\frac{1}{2} P_1 (D_x^{\ 2} + D_z^{\ 2}) - P_2 D_x] D_x x \\ &+ \frac{1}{2} (D_x^{\ 2} + D_z^{\ 2}) P_2 x - P_4 D_x x + P_5 D_z x + \left(\frac{1}{S} + \frac{1}{H}\right) D_x x = (n - \frac{1}{2})\lambda \end{aligned} \tag{43}$$

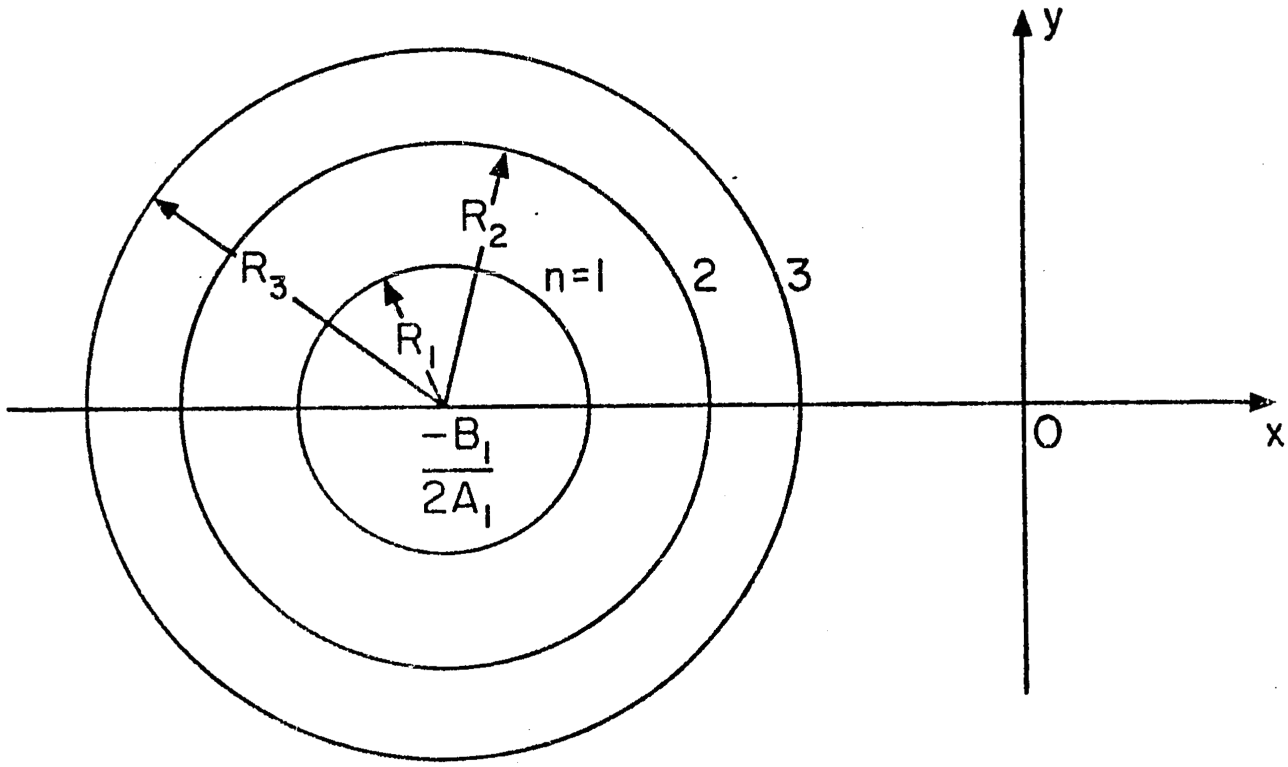


Figure 4. Loci of fringes for $D_z \neq 0$, and $D_x = D_y - 0$.

Rearranging terms, we have

$$y = \pm \{\frac{1}{2} P_1 D_x x^3 - \frac{1}{2} [P_2 D_x + P_3 D_z - \frac{1}{2} P_1 (D_x^2 + D_z^2) - (\frac{1}{2} P_1 D_z^2 + P_2 D_x)] x^2$$

$$- [\frac{1}{2} (3D_x^2 + D_z^2) P_2 - P_4 D_x + P_5 D_z - (\frac{1}{S} + \frac{1}{H}) D_x] x$$

$$+ (n - \frac{1}{2}) \lambda\}^{1/2} / (\frac{1}{2})^{1/2} [P_2 D_x + P_3 D_z - \frac{1}{2} P_1 (D_x^2 + D_z^2) - P_1 D_x x]^{1/2} . \quad (44)$$

Equation (44) indicates that for any given ($D_x$, 0, $D_z$), a relationship between y and z can be computed and the loci of the fringes can then be determined.

Case (iii). When $D_x = 0$, $D_y \neq 0$, and $D_z \neq 0$ are substituted into Eq. (32), it becomes

$$- \frac{1}{2} P_1 D_y y x^2 - \frac{1}{2} P_1 D_y y^3 + \frac{1}{2} [P_3 D_z - \frac{1}{2} P_1 (D_y^2 + D_z^2)] x^2$$

$$+ \frac{1}{2} [P_3 D_z - \frac{1}{2} P_1 (3D_y^2 + D_z^2)] y^2 - P_2 D_y y x + (\frac{1}{S} + \frac{1}{H}) D_y y$$

$$- \frac{1}{2} P_1 (D_y^2 + D_z^2) D_y y + [\frac{1}{2} (D_y^2 + D_z^2) P_2 + P_5 D_z] x$$

$$- (n - \frac{1}{2}) \lambda = 0 . \quad (45)$$

Rearranging the terms in Eq. (45);

$$\frac{1}{2} [P_1 D_y y - P_3 D_z + \frac{1}{2} P_1 (D_y^2 + D_z^2)] x^2 + [P_2 D_y y - \frac{1}{2} (D_y^2 + D_z^2) P_2 - P_5 D_z] x$$

$$+ \frac{1}{2} \{P_1 D_y y^3 - [P_3 D_z - \frac{1}{2} P_1 (3D_y^2 + D_z^2)] y^2 + (\frac{1}{S} + \frac{1}{H}) D_y y$$

$$+ P_1 (D_y^2 + D_z^2) D_y y - (2n - 1) \lambda\} = 0 . \quad (46)$$

If one lets

$$A(y) = \frac{1}{2}\,[P_1 D_y y - P_3 D_z + \frac{1}{2} P_1 (D_y{}^2 + D_z{}^2)]\ , \tag{47}$$

$$\quad = P_2 D_y y - \frac{1}{2}\,(D_y{}^2 + D_z{}^2)\ P_2 - P_5 D_z\ , \tag{48}$$

$$C(n,y) = \frac{1}{2}\,\{P_1 D_y y^3 - [P_3 D_z - \frac{1}{2} P_1\ (3D_y{}^2 + D_z{}^2)]\ y^2 + (\frac{1}{S} + \frac{1}{H}) D_y y + P_1 (D_y{}^2 + D_z{}^2)\ D_y y + (2n - 1)\ \lambda\}\ , \tag{49}$$

then Eq. (46) may be rewritten as

$$A(y)x^2 + B(y)x + C(n,y) = 0\ . \tag{50}$$

The solution of the above quardratic equation gives

$$x = \frac{-B(y) \pm \sqrt{B^2(y) - 4A(y)C(n,y)}}{2A(y)}\ . \tag{51}$$

Theoretically, for a given set of $(0, D_y, D_z)$ and n, due to the ± signs in Eq. (51) a pair of points (x,y) may be found. The collection of these points will enable one to graphically express the loci of the interference fringes.

Apparently, all these equations are too complicated to compute and simplifications by appropriate approximations are highly desirable, or even necessary, to make the model practical. This will be done below.

B. An Approximate Model for Simple Translations

Under certain conditions, the model given by Eq. (32) can be directly simplified to a state which will more clearly reveal physical meanings than the original model.

$$A_2 \equiv \frac{1}{2} D_z\left(\frac{\sin\theta_S}{S^2} + \frac{\sin\theta_H}{H^2}\right) , \tag{54}$$

$$B_2 \equiv D_z\left(\frac{\sin\theta_S \cos\theta_S}{S} - \frac{\sin\theta_H \cos\theta_H}{H}\right) + D_x\left(\frac{1}{S} + \frac{1}{H}\right) , \tag{55}$$

and

$$C_2 \equiv D_y\left(\frac{1}{S} + \frac{1}{H}\right) . \tag{56}$$

When Eqs. (54), (55) and (56) are substituted into Eq. (53), it becomes

$$A_2(x^2 + y^2) + B_2 x + C_2 y = (n - \frac{1}{2}) \lambda , \tag{57}$$

or

$$\left(x + \frac{B_2}{2A_2}\right)^2 + \left(y + \frac{C_2}{2A_2}\right)^2 = \frac{1}{4A_2^2} [B_2^2 + C_2^2 + 4A_2(n - \frac{1}{2}) \lambda] . \tag{58}$$

The above equation indicates that the fringe loci form concentric circles with center located at $(x_C, y_C)$ where

$$x_C = \frac{-B_2}{2A_2} = [D_z \sin\theta_S \cos\theta_S \left(\frac{1}{H} - \frac{1}{S}\right) - D_x\left(\frac{1}{S} + \frac{1}{H}\right)] / [D_z\left(\frac{\sin\theta_S}{S^2} + \frac{\sin\theta_H}{H^2}\right)] . \tag{59}$$

and

$$y_C = \frac{-C_2}{2A_2} = -\frac{D_y}{D_z}\left(\frac{1}{S} + \frac{1}{H}\right) / \left(\frac{\sin\theta_S}{S^2} + \frac{\sin\theta_H}{H^2}\right) . \tag{60}$$

The radius of the locus of the $n^{th}$ fringe may be written as

$$R_n = \left(\frac{1}{2A_2}\right) [B_2^2 + 4A_2(n - \frac{1}{2}) \lambda]^{1/2} . \tag{61}$$

PRECEDING PAGE BLANK NOT FILMED

From Eq. (60), for any given value of $D_z$, $y_C$ is proportional to $D_y$ and $y_C = 0$ if $D_y = 0$. In addition, the radius $R_n$ given by Eq. (61) shows that for large values of n, $R_n$ is proportional to $\sqrt{n}$, a feature shared by the fringes of the Fresnel zone plate.

For the purpose of comparing the degree of accuracy of this approximate model with the experimental data, a computer program was written to calculate Eqs. (59), (60) and (61). This program together with the computed results of $(x_C, y_C)$ and $R_n$ in terms of n, $D_x$, $D_y$, $D_z$, S, H, $\theta_S$, and $\theta_H$ are included in Appendix D.

Finally, when n is very large, the spacing between any two neighboring circular fringes can be measured to help determine the amount of displacement. Therefore, the following equation, deduced from Eq. (61) may be needed in this case,

$$\begin{aligned} d_{n,n+1} &= R_{n+1} - R_n \\ &= \left(\frac{1}{2A}\right)\{[B^2 + C^2 + 4A(n + \tfrac{1}{2})\ \lambda]^{1/2} \\ &\quad - [B^2 + C^2 + 4A(n - \tfrac{1}{2})\ \lambda]^{1/2}\}\ . \end{aligned} \tag{62}$$

C. The Treatment of Rotations and Translations

When a rotation-type displacement represented by $\vec{\omega}$ happens after a translation $\vec{D}_t$ of a point p(x,y) is made between the two exposures of the hologram, the diagram shown in Fig. 2 needs to be modified. The new configuration is shown in Fig. 5 with the vectors $\vec{t}$, $\vec{R}$, $\vec{D}_t$, and $\vec{\omega}$ denoted.

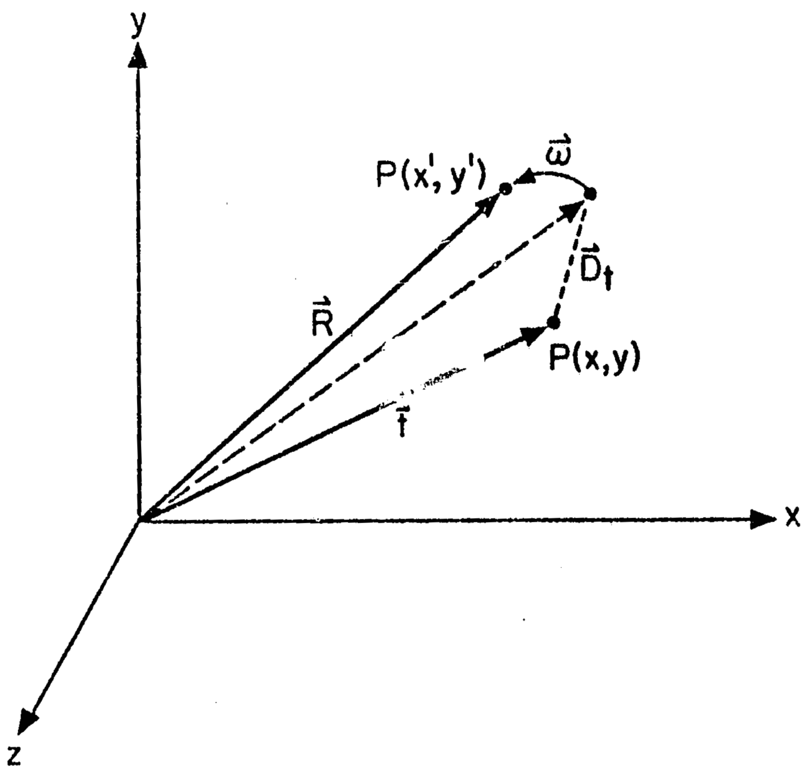


Figure 5. A rotation of $\vec{\omega}$ after the translation $\vec{D}_t$ bringing P(x,y) to P(x',y').

A rotation around the x-axis with an angle $\omega_x$ will give rise to a displacement vector $\vec{D}_{\omega_x}$, which can be written as

$$\vec{D}_{\omega_x} = y(\cos \omega_x - 1)\,\hat{j} + y \sin \omega_x\,\hat{k} \,. \tag{63}$$

Similarly, a rotation around the y-axis of an angle $\omega_y$ will yield

$$\vec{D}_{\omega_y} = x(\cos \omega_y - 1)\,\hat{i} - x \sin \omega_y\,\hat{k} \,, \tag{64}$$

and a rotation around the z-axis will produce

$$\vec{D}_{\omega_z} = [x(\cos \omega_z - 1) - y \sin \omega_z]\,\hat{i}$$

$$+ [y(\cos \omega_z - 1) + x \sin \omega_z]\,\hat{j} \,. \tag{65}$$

From Eqs. (63), (64) and (65), it may be concluded that simple rotations may be treated equivalently as translations and either Eq. (32) or (58) may used to describe the loci produced by these rotations.

In case that the displacements are in the form of a combination of rotations with translations of $\vec{D}_t = D_x\,\hat{i} + D_y\,\hat{j} + D_z\,\hat{k}$, the net displacement vector may be written as:

$$\vec{D}_{D_t,\omega_x} = D_x\,\hat{i} + [y(\cos \omega_x - 1) + D_y \cos \omega_x]\,j$$

$$+ [(y + D_y) \sin \omega_x + D_z]\,\hat{k} \,, \tag{66}$$

for $\vec{D}_t$ and $\vec{\omega} = \omega_x\,\hat{i}$.

Likewise,

$$\vec{D}_{D_t,\omega_y} = [x(\cos\,\omega_y - 1) + D_x \cos\,\omega_y]\,\hat{i}$$

$$+ D_y\,\hat{j} - [(x + D_x)\sin\,\omega_y - D_z]\,\hat{k}\ , \tag{67}$$

for $\vec{D}_t$ and $\vec{\omega} = \omega_y\,\hat{j}$ , and

$$D_{D_t,\omega_z} = [x(\cos\,\omega_z - 1) - y\sin\,\omega_z + D_x \cos\,\omega_z$$

$$- D_y \sin\,\omega_z]\,\hat{i}$$

$$+ [y(\cos\,\omega_z - 1) + x\sin\,\omega_z + D_y \cos\,\omega_z$$

$$+ D_x \sin\,\omega_z]\,\hat{j}$$

$$+ D_z\,\hat{k} \tag{68}$$

for $\vec{D}_t$ and $\vec{\omega} = \omega_z\,\hat{k}$.

A good approximation can be made as follows. In the region where $x >> D_z$, $y >> D_y$, and $z >> D_z$ (these inequalities are generally valid almost everywhere since D is assumed to be extremely small), Eqs. (66), (67) and (68) become respectively

$$\vec{D}_{D_t,\omega_y} = D_x\,\hat{i} + y(\cos\,\omega_x - 1)\,\hat{j} + (y\sin\,\omega_x + D_z)\,\hat{k}\ , \tag{69}$$

$$\vec{D}_{D_t,\omega_y} = x(\cos\,\omega_y - 1)\,\hat{i} + D_y\,\hat{j} + (D_z - x\sin\,\omega_y)\,\hat{k}\ , \tag{70}$$

and

$$\vec{D}_{D_t,\omega_z} = [x(\cos \omega_z - 1) - y \sin \omega_z] \hat{i}$$

$$+ [y(\cos \omega_z - 1) + x \sin \omega_z] \hat{j} + D_z \hat{k} , \qquad (71)$$

Once again, in the calculations of the fringe loci, either Eqs. (69), (70) or (71) may be used with either Eq. (32), the unabridged version of the model, or Eq. (58), the simplified model, depending on the particular situation.

## III. EXPERIMENT

The experimental set-up and procedure have been described in detail in a previous report[19], therefore, only a brief discussion will be included. The realization of the CMHNDT system is shown in Fig. 6. A 10-watt CW Argon ion laser (Spectra Physics Model 170) is used as a major light source. Two small 1-mW He-Ne lasers are used for the construction of two separate Michelson interferometers, which are used for an accurate monitor of the micrometer controlled displacement. Instead of the mock-up of the rocket in the Figure, the test plate is placed on a Weiser/Robodyne Model 119 micrometer translation stage. The smallest scale of the micrometer head has a reading of 2.54 μm. Small mirrors are mounted on the sides of the test plate for the construction of the Michelson interferometers. The test plate, translation stage and one of the small mirrors are shown in Fig. 7.

The basic idea of the experimental set-up is to use an optical system (Michelson interferometer) to monitor a mechanical system (the test plate and translation stage combination) for the purpose of the calibration of the optical CMHNDT system. The procedure is to take double-exposure holograms with different incident angles, displacements of the plate and a variety of curve plates so that the model derived in the last Section may be tested and consequently the CMHNDT

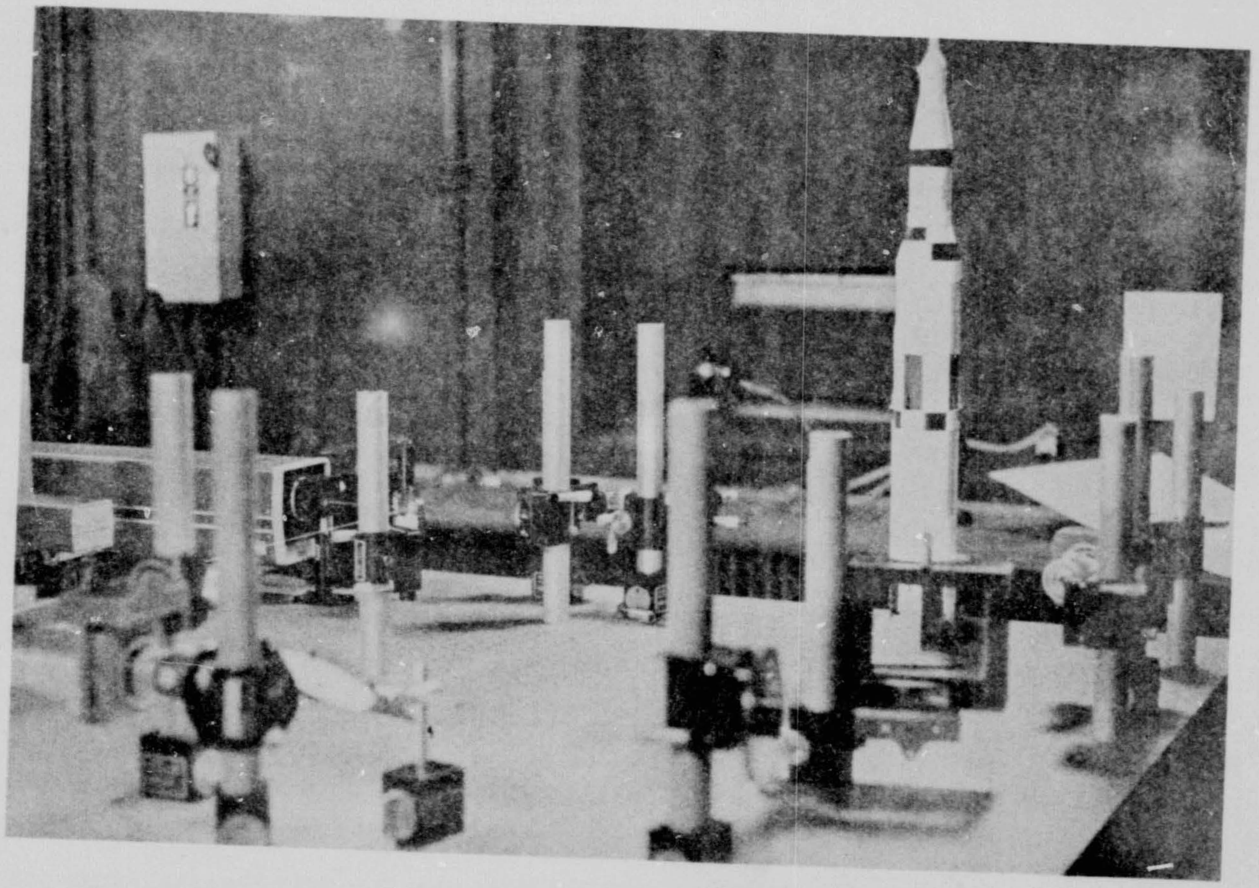

Figure 6. The CMHNDT system realization.

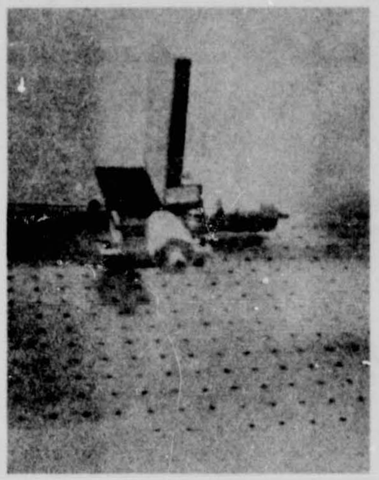

(a) Side-view of the plate and the translation stage.

(b) The small mirror is visible in the center of the plate.

Figure 7. The test plate mounted on the translation stage.

system may be evaluated. Representative experimental results are presented below.

The configuration of the CMHNDT system as shown in Fig. 1 is designed with $S = 92$ cm, $H = 38$ cm, and variable values of $\theta_S$ and $\theta_H$. The dimensions of the flat test plate are 13 cm x 16 cm x 2.54 cm. When $\theta_S = \theta_H = 73.5°$, a sequence of double exposure holograms have been recorded for $D_y = D_z = 0$ and $D_x = 5.08$, 10.16, 15.24 and 20.32 μm. The corresponding real images are shown as photographs in Fig. 8. Likewise, photographs of double-exposure holograms with $D_x$ and $D_z$ translations and with $D_y = 0$ are shown in Fig. 9.

In addition to the flat test plate, test plates with a cylindrical shape of radii of 20.32 cm (8"), 15.24 cm (6"), and 10.16 cm (4") have also been used. A series of photographs of double exposure holograms with $S = 66.5$ cm, $H = 45$ cm, $\theta_H = 75°$, $\theta_S = 75°$, 60°, 45°, and 30°, and $D_x = D_y = 0$, $D_z = 25.4$, 38.1, 50.8, and 63.5 μm have been obtained. The results are shown in Figures 10 through 13. The horizontal and vertical scale on the photographs in these Figures are 2 cm/division.

The analysis of the photographs in this Section and the comparison of the experimental results with theory will be given in the next Section.

## IV. COMPARISON OF THE THEORY AND THE EXPERIMENT

From the experimental data presented in the last Section, a few special cases of the theory in Section II may be tested to see how valid they are. They are (i) Axial translations, i.e. varying $D_x$ or $D_z$, (ii) Oblique translations, i.e., varying $D_x$ and $D_z$, and (iii) Incident angle effect, i.e. varying $D_x$ and the angle $\theta_S$. In addition, the relationship between the curvature of the test plate and the system may also be observed through the data in

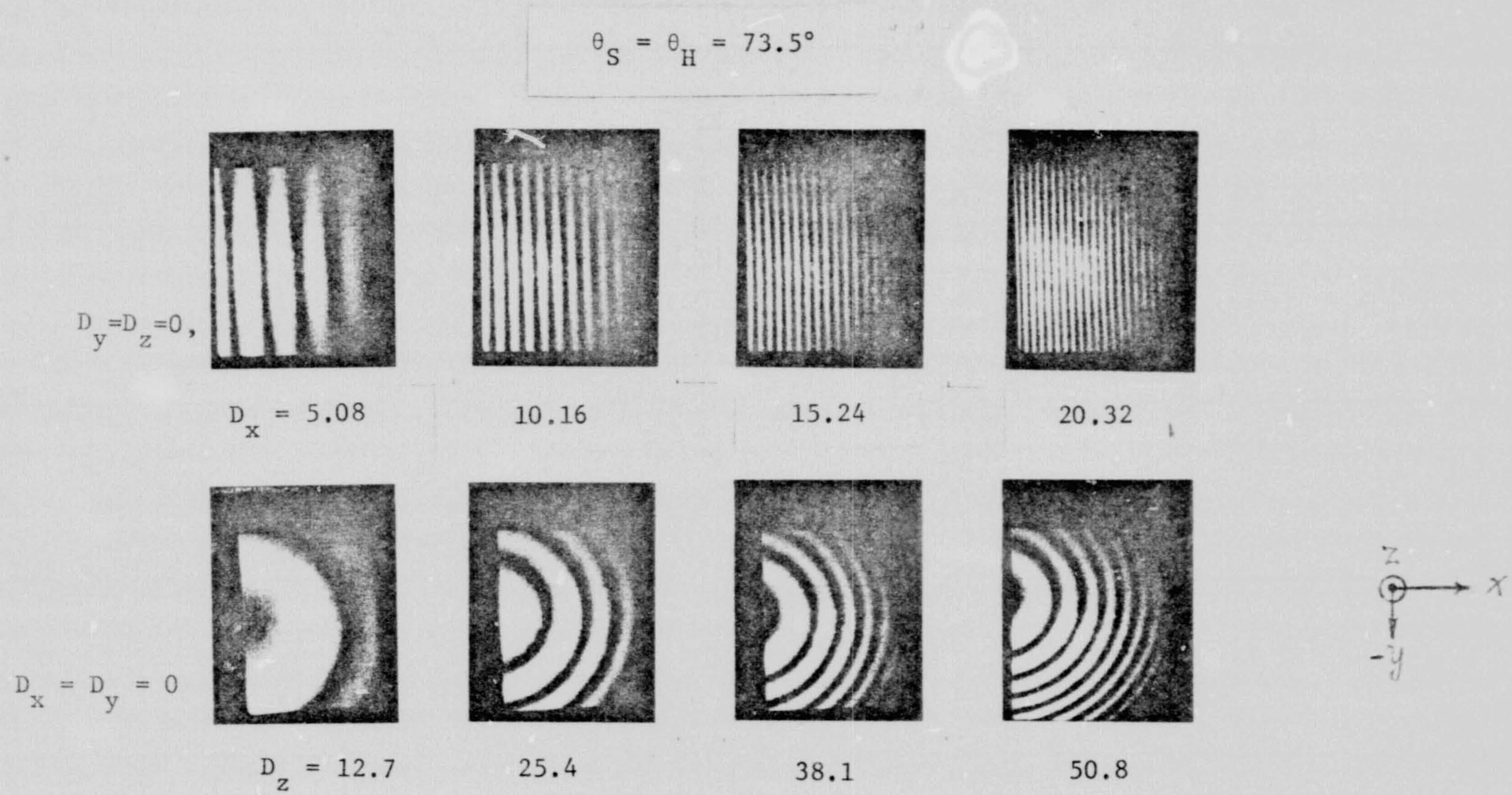


Figure 8 . Photographs of real images of double-exposure holograms for displacements along x-axis (top row) and along z-axis (bottom row). All units are in micrometers.

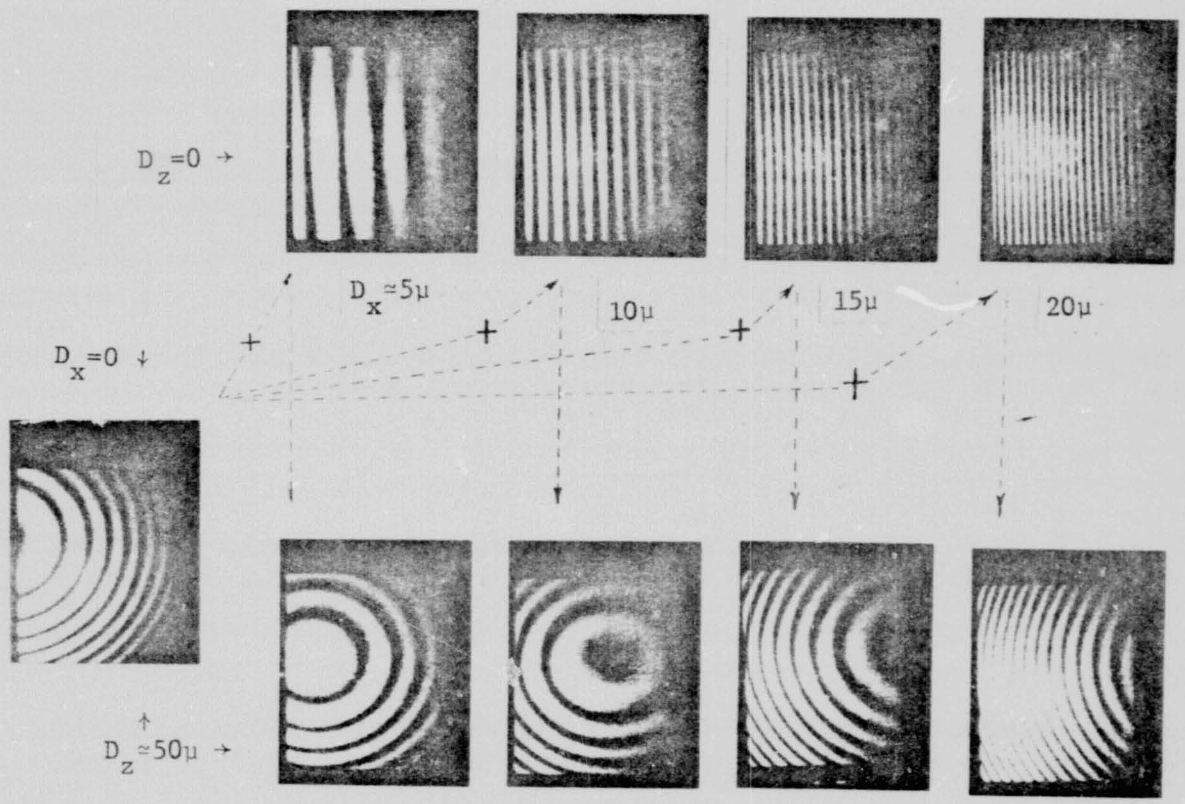


Figure 9 . A systematic presentation of the object performing axial translations and oblique translations on the fringe patterns.

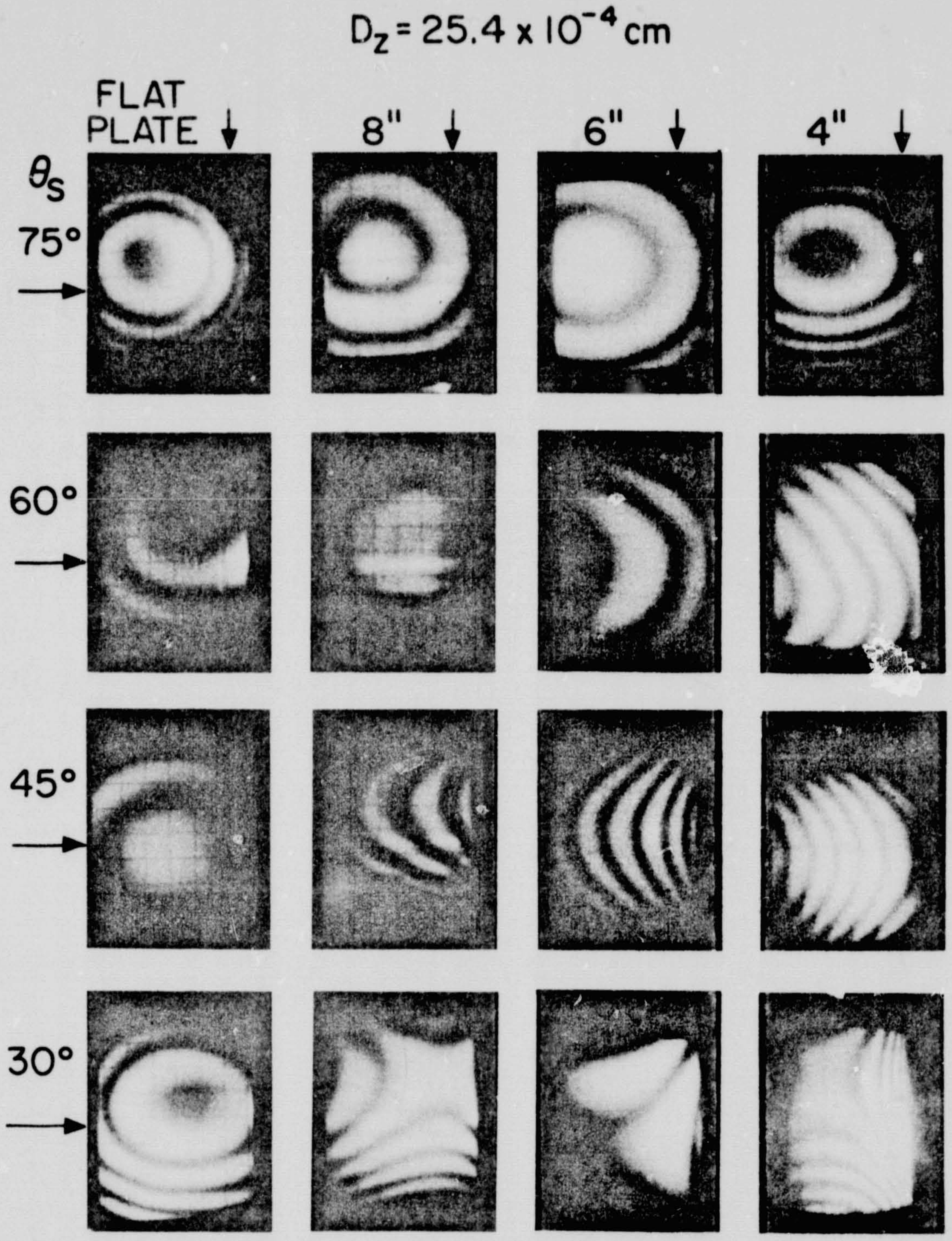




Figure 10 Photographs of real images of double-exposure holograms of flat and curve plates at different $\theta_s$ and for $D_z$=25.4 μm

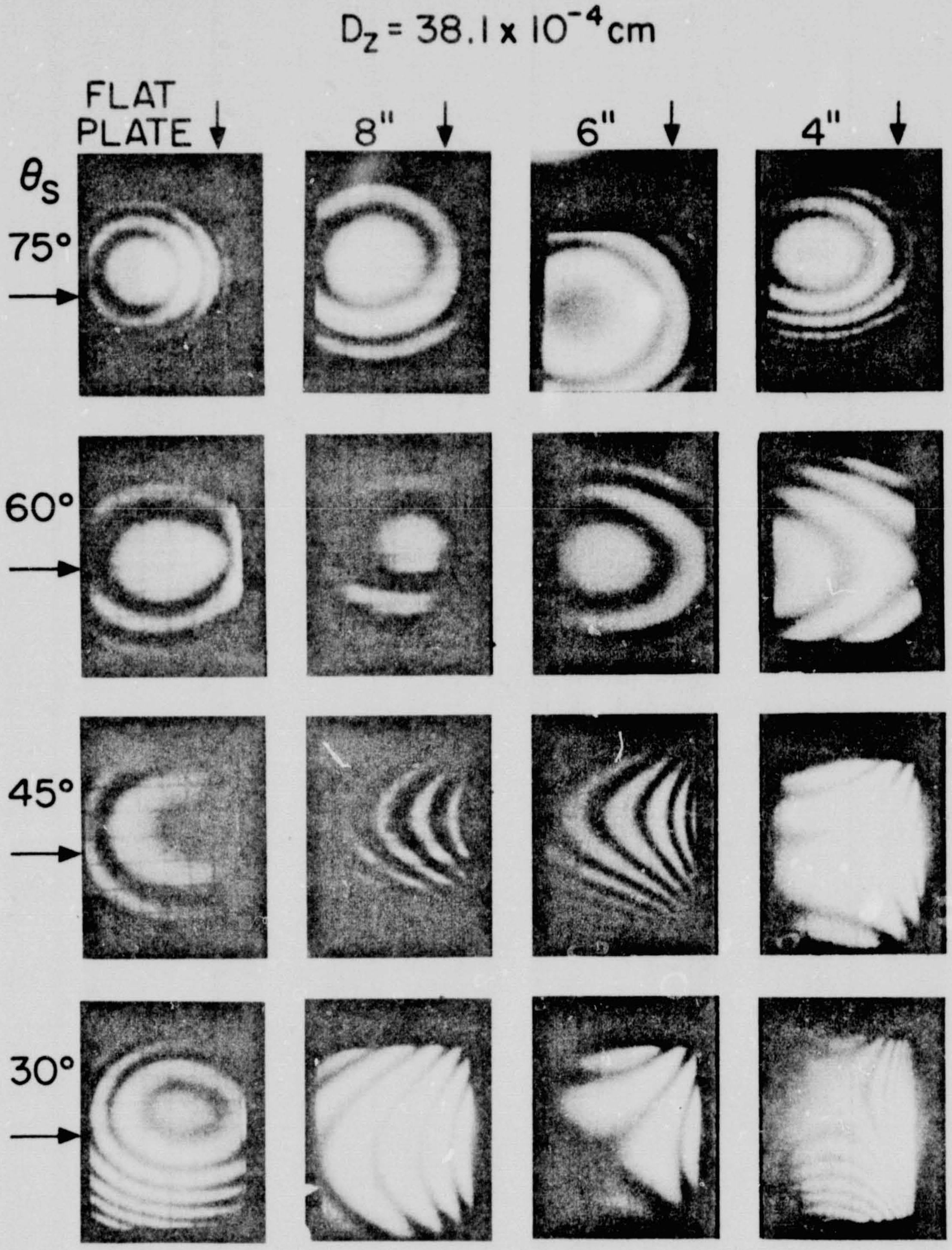


**Figure 11** Photographs of real images of double-exposure holograms of flat and curve plates at different $\theta_S$ and for $D_z$=38.1 μm.

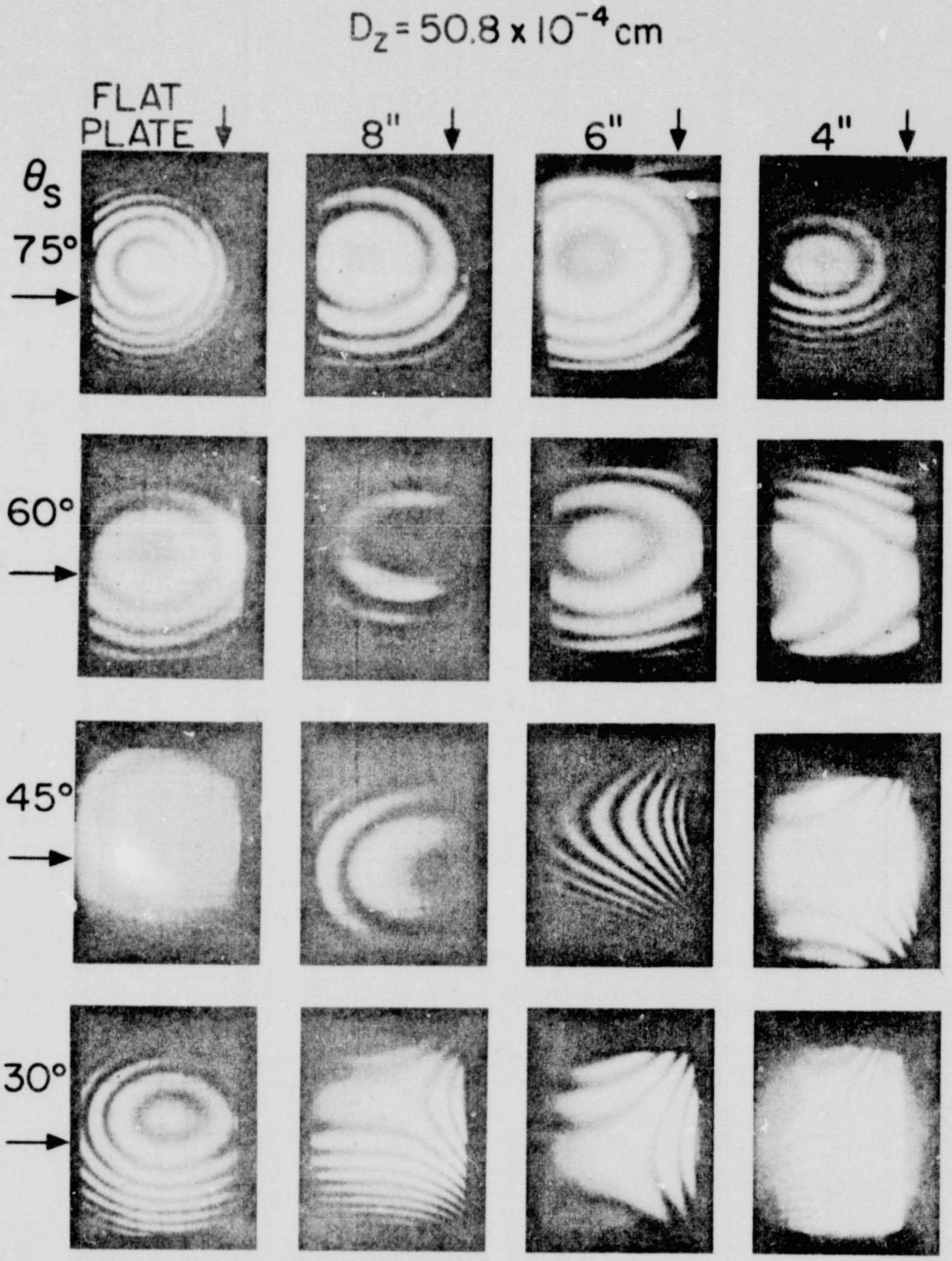


Figure 12 Photographs of real images of double-exposure holograms of flat and curve plates at different $\theta_s$ and for $D_z$=50.8 µm.

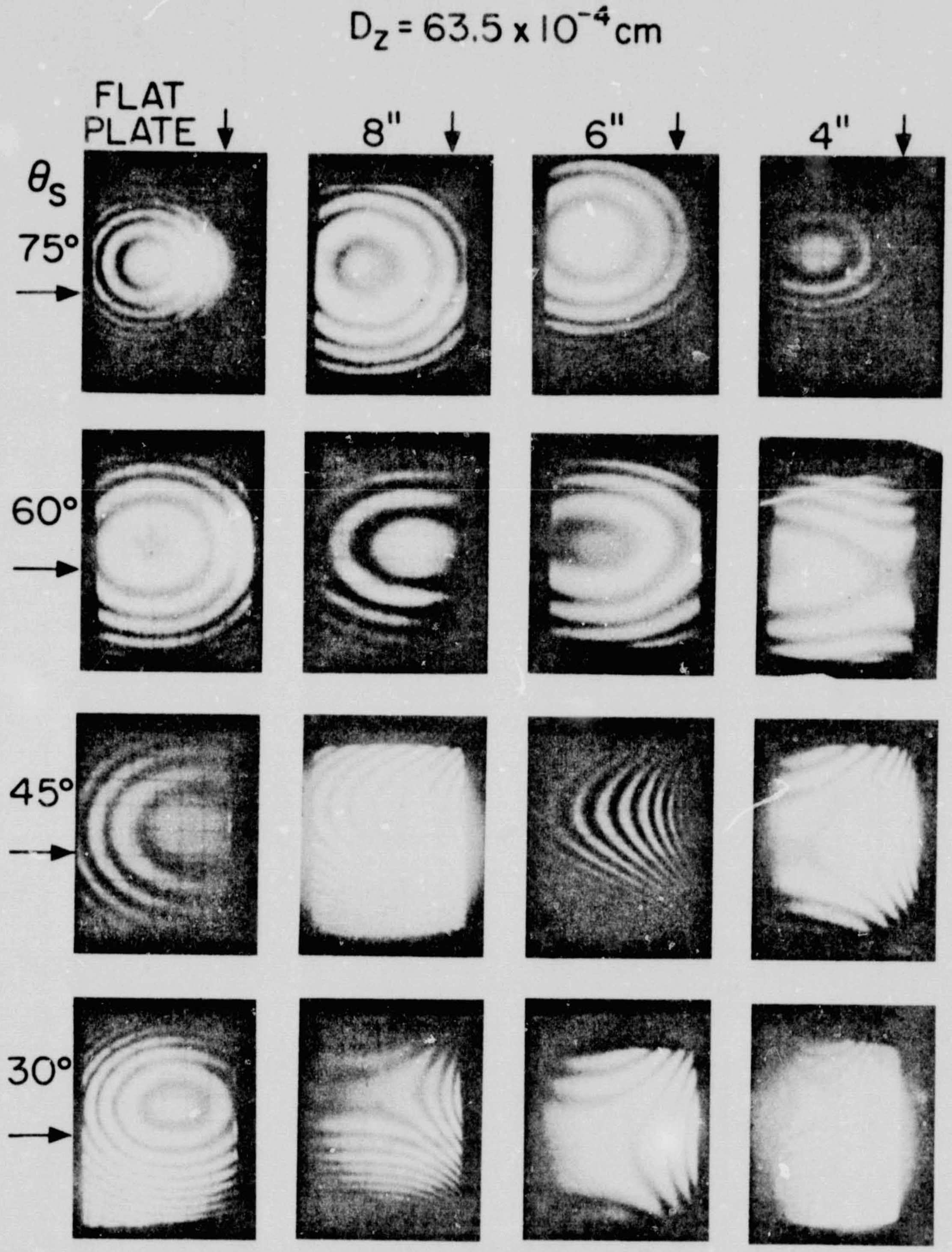


Figure 13 Photographs of real images of double-exposure holograms of flat and curve plates at different $\theta_S$ and for $D_z$=63.5 μm.

Figures 10-13. Details of the analysis are described below.

Case (i). Axial translations. There are two subcases:

Subcase (iA) $D_y = D_z = 0$, $D_x$ is varying:

The typical experimental results can be represented by the photographs in Fig. 8. The parameters pertaining to this experiment are

$$\theta_H = \theta_S = 73.5°$$

$$S = 92 \text{ cm}$$

$$H = 38 \text{ cm}$$

$$\lambda = 0.5145 \times 10^{-4} \text{ cm}, \tag{72}$$

From the first order theory, consisting of Eqs. (22), (23), and (24), the spacing between any two adjacent fringes is obtained as

$$\Delta x = \lambda/\left[D_x\left(\frac{1}{S} + \frac{1}{H}\right)\right]. \tag{73}$$

For example, when $D_x = 5.08 \times 10^{-4}$ cm and $\frac{1}{S} + \frac{1}{H} = 0.0372$ $(\frac{1}{\text{cm}})$, $\Delta x = 2.72$ cm was obtained.

The experimental data may be obtained by dividing the width of the plate (13 cm) by the total number of fringes across the plate (see the top row of Fig. 8). For instance, when $D_x = 5.08$ μm, there are approximately 4.5 fringes, hence $\Delta x = 13$ cm/4.5 = 2.89 cm. Following the example, Eq. (73) and the data in Fig. (8), Table I is established for the comparison of the theory to the experiment.

Table I. Comparison between theory and experiment of the fringe spacing $\Delta x$ for $D_x \neq 0$, $D_y = D_z = 0$.

| $D_x$ (μm) | Exp. $\Delta x$ (cm) | Th. $\Delta x$ (cm) |
|---|---|---|
| 5.08 | 2.89 | 2.72 |
| 10.16 | 1.37 | 1.36 |
| 15.24 | 0.87 | 0.91 |
| 20.32 | 0.65 | 0.68 |

From the results of this case, it is obvious that there is a reasonable agreement between the theory and experiment.

Subcase (iB), $D_x = D_y = 0$, $D_z$ is varying:

From the theory, Eqs. (54) through (57), and Eq. (72) may be applied and one finds that $C = 0$, $y_C = 0$, and

$$A = \frac{1}{2}\left(\frac{\sin 73.5°}{(92)^2} + \frac{\sin 73.5°}{(38)^2}\right) D_z = 3.89 \times 10^{-4} D_z$$

$$B = \left(\frac{\sin 73.5° \cos 73.5°}{92} - \frac{\sin 73.5° \cos 73.5°}{38}\right) D_z$$

$$= (2.96 \times 10^{-3} - 7.17 \times 10^{-3})\, D_z$$

$$= -4.21 \times 10^{-3}\, D_z \ .$$

From Eq. (59),

$$x_C = -B/2A = 5.41 \text{ cm} . \tag{74}$$

In addition, by substituting n = 1 and $D_z$ = 12.7 μm into Eq. (61), the radius of the first circular fringe $R_1$ is found to be

$$R_1 = [(\frac{B}{2A})^2 + (n - \frac{1}{2}) \frac{\lambda}{A}]^{1/2}$$

$$= [(5.41)^2 + \frac{\frac{1}{2} \times 0.5145 \times 10^{-4}}{3.49 \times 10^{-4} \times 12.7 \times 10^{-4}}]^{1/2}$$

$$= 9.34 \text{ cm} ,$$

The radii for other values of $D_z$ can likewise be found. The experimental data can be extracted from the bottom row of Fig. 8. A comparison between these data is listed in Table II.

Table II. Comparison between the theoretical and experimental values of $R_1$ for $D_x = D_y = 0$, $D_z \neq 0$.

| $D_z$ (μm) | Exp. $R_1$ (cm) | Th. $R_1$ (cm) |
|---|---|---|
| 12.7 | 7.62 | 9.34 |
| 25.4 | 6.02 | 7.63 |
| 38.1 | 5.08 | 6.97 |
| 50.8 | 4.32 | 6.62 |

Again the agreement between theory and experiment is quite close.

Case (ii). Oblique translations:

The experimental parameters for the oblique translations are the same as those in Case (i). In this case, $D_y = 0$ but $D_x \neq 0$ and $D_z \neq 0$ so that the translation is oblique to the perpendicular of the plate. The experimental result is shown in Fig. 9. It is interesting to note that the center of the concentric circular-shaped fringes has been shifted along the x-axis. For the theoretical interpretation of the result, Eqs. (54) through (61) of the simple model are employed.

From Eq. (54),

$$A_2 = 3.87 \times 10^{-4} D_z \tag{75}$$

and Eq. (55),

$$B_2 = -4.21 \times 10^{-3} D_z + 37.5 \times 10^{-3} D_x \tag{76}$$

The center of the fringes is predicted to be at

$$x_C = 5.41 - 48.04 \frac{D_x}{D_z} , \tag{77}$$

and

$$y_C = 0. \tag{78}$$

The comparison between the theory and experiment for $x_C$ is shown in Table III.

Table III. Comparison of the theoretical and experimental values of $x_C$ for $D_y = 0$ and $D_z = 50.8$ μm.

| $D_x$ (μm) | Exp. $x_C$ (cm) | Th. $x_C$ (cm) | (Exp. $x_C$ - Th. $x_C$) (cm) |
|---|---|---|---|
| 0 | 9 | 5.41 | 3.59 |
| 5.08 | 3.81 | 0.61 | 3.2 |
| 10.16 | -1.4 | -4.20 | 2.8 |
| 15.24 | -7 | -9.00 | 2.0 |
| 20.32 | -12 | -13.81 | 1.81 |

The above table shows a discrepancy of 1.8 to 3.6 cm between the experimental data and their theoretical counterpart. The errors might result from the fact that the experimental data were taken from the center of the plate, which may turn out to be not the true center of the coordinate system of the fringes. If a calibration system in the form of the flat plate is used, this problem can be handled in a controlled manner.

Case (iii). The effect of the incident angle $\theta_S$ on the interference fringes: In order to see the effect of the variation of $\theta_S$ on the double-exposure interference fringes, other parameters have been set at $\theta_H = 75°$, H = 45 cm, S = 66.5 cm, and $D_x = D_y = 0$. The displacement $D_z$ has values of 12.7 μm, 25.4 μm, 38.1 μm, 50.8 μm, and 63.5 μm. Theoretical values of the fringe loci based on Eqs. (54) through (61) are calculated corresponding to these parameters with the help of a computer program as shown in Appendix D. Experimental data are obtained from Fig. 10 to Fig. 13.

The comparison between the theoretical and experimental values for the centers of the loci of the fringes ($x_C$, $y_C$), for the flat test plate, is shown in Table IV. It can be seen that the centers vary as the angle $\theta_S$ and $D_z$ vary, although not of any significant degree.

Table IV. Comparison of the centers of the loci ($x_C$,$y_C$) between experiment and theory for various $\theta_S$ and $D_z$. The flat plate is used. Other parameters are $\theta_H$ = 75°, H = 45 cm, S = 66.5 cm, $D_x$ = 0, and $D_y$ = 0.

| $\theta_S$(°) / $D_z$($10^{-4}$cm) | 30° | 45° | 60° | 75° |
|---|---|---|---|---|
| 12.7 | (-0.4, 1) | | (-1.0, 2) | (1, .3) |
| 25.4 | (-1.2, 1) | (-0.4, .2) | (-1.5, 3) | (2.2, 1) |
| 38.1 | (-1, 1) | (-2.1, .2) | (0, 0.4) | (2.2, 1) |
| 50.8 | (-0.8, 1.2) | | (1.0, 0.2) | (2.1, 1) |
| 63.5 | (-1, 1.2) | (-3.6, 0) | (1.0, -0.25) | (1, 1) |
| Theory | (-1.62, 0) | (-3.1, 0) | (-1.42, 0) | (2.58, 0) |

Note 1: Experimental ($x_C$, $y_C$) is measured from the center of the test plate.

Note 2: The units are in centimeters.

These variations can be attributed to the fact that the experimentally measured coordinates of the centers have been based on the center of the test plate as the origin, which again may not be an exact origin. In addition, minute experimental uncertainties such as the possible displacements along the x- and y-direction during the translations along the z-direction can also cause the center to shift, similar to the results described in the previous cases. Moreover, the laser light expanded by the spatial filter are not perfect spherical waves as assumed in the theory.

The radii of the loci for $\theta_S = 75°$ and the various values of $D_z$ are shown in Table V.

In Table V, T indicates the theoretical values, which are found from the output of the computer program listed in Appendix D. Two experimental data for each radius are presented to indicate that the loci observed are often not perfect circles, but are more or less of elliptical shapes. The symbol in the table represents the coordinate value where the locus intercepts the vertical axis; and H, the horizontal axis. The fact that the loci observed are not perfect circles may be caused also by the fact that the light source expanded by the spatial filter is not a perfect spherical wave as it was assumed in the theory. Of course, the approximation used could also contribute a small amount to the effect because the high order terms have been neglected. However, the first reason seems stronger since the tendency of the locus toward an elliptical shape increases as the incidence angle $\theta_S$ becomes smaller, i,e., a more slanted incidence of the light. This point is clear from the comparison of the fringes on the flat plate with different incident angles $\theta_S$ in Figs. 10, 11, 12 and 13. The blanks in the Table represent that the data are indeterminable from the photograph.

Table V. Comparison between theory and experiment for the radii of the fringe loci of the flat plate for $\theta_S = 75°$, $\theta_H = 75°$, H = 45 cm, S = 66.5 cm, $D_x = 0$ and $D_y = 0$.

$\theta_S = 75°$

| $D_z (10^{-4}$ cm) | $R_n$ (cm) | $R_1$ | $R_2$ | $R_3$ | $R_4$ | $R_5$ |
|---|---|---|---|---|---|---|
| 12.7 | V | 5.6 | 9.2 | | | |
| | H | 6.2 | | | | |
| | T | 7.87 | 13.1 | 16.8 | 19.8 | 24.4 |
| 25.4 | V | 5 | 6.8 | 8.4 | | |
| | H | 5 | 7 | 8.6 | | |
| | T | 5.86 | 9.46 | 12.0 | 14.1 | 16.0 |
| 38.1 | V | 4.0 | 5.6 | 6.6 | 7.6 | |
| | H | 4.4 | 6.0 | 7.2 | 8.4 | |
| | T | 5.01 | 7.87 | 9.94 | 11.6 | 13.1 |
| 50.8 | V | 3.2 | 4.6 | 5.8 | 6.6 | 7.6 |
| | H | 3.2 | 5 | 6 | 7 | 7.8 |
| | T | 4.52 | 6.94 | 8.70 | 10.2 | 11.4 |
| 63.5 | V | 3 | 4.2 | 5.0 | 6.0 | 6.6 |
| | H | 3 | 4.4 | 5.6 | 6.2 | 7 |
| | T | 4.21 | 6.31 | 7.87 | 9.17 | 10.3 |

V: Vertical (Expt.)

H: Horizontal (Expt.)

T: Theoretical

In order to demonstrate the comparison between the theory and the experiment in a more illuminating form, the experimental and theoretical radii are plotted with results shown in Figs. 14 through 16. The arithmetic average of V and H is taken as an equivalent radius of an imagined circular locus, which can be compared more easily with the theoretical values.

Similarly, when $\theta_S = 60°$, the comparisons are shown by Table VI and Figures 17, 18 and 19; when $\theta_S = 45°$, the comparisons are shown by Table VII and Fig. 20; $\theta_S = 30°$, by Table VIII and Figures 21, 22 and 23.

On close examination of the data for each $\theta_S$, a common feature emerges. From Figures 14 through 16, it can be seen that the experimental "radii" are consistently smaller than the theoretical radii. Figures 17 through 19 show smaller discrepancies between theory and experiment; Fig. 20 shows that the experimental data are larger than the theoretical data; and Figs. 21 through 23 show that the theoretical data are again larger than the experimental data. Nevertheless, the discrepancies are in all events small. These discrepancies can be justifiably attributed to the fact that it is rather difficult to determine the fringe contrast, and hence the exact values of the radii, and therefore errors in the readings of the radii from the photographs consequently occurred.

Finally, it should be noted that an important phenomenon concerning the relationship between the incident angle $\theta_S$ and the surface curvature of the test plate is revealed by the photographs in Figs. 10 through 13. It seems that when the incident angle $\theta_S = 75°$, the discrepancies between the loci of the flat plate and the plates of cylindrical shaped surfaces (the outer surfaces of the cylinders are used) of radii of 20.32 cm (8 in), 15.24 cm (6 in), and 10.16 cm (4 in) are relatively small. When the angle varies from $\theta_S = 75°$ to $\theta_S = 60°$, 45°, and 30°, the discrepancies begin to increase significantly with the reduction

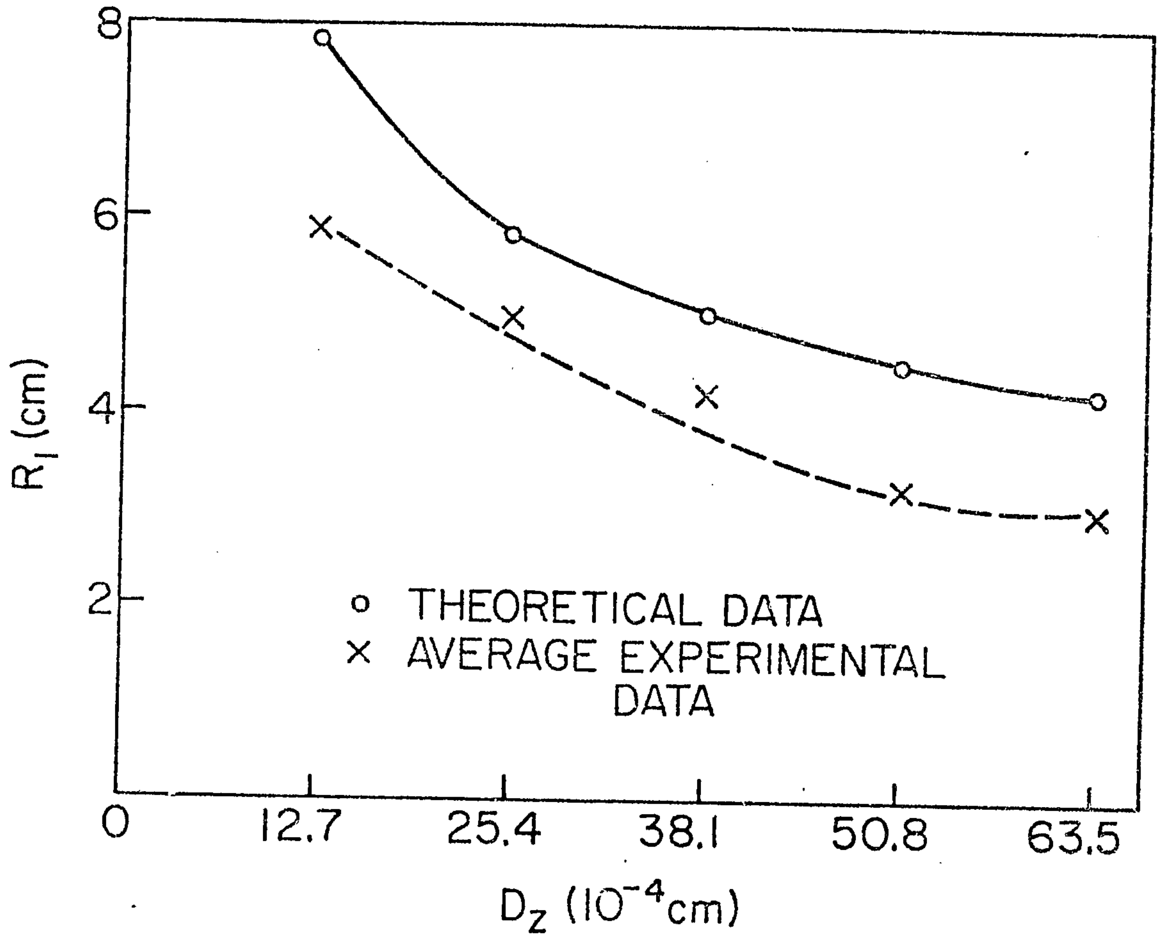


Figure 14 Comparison between the theoretical and the average experimental data for $D_z$ versus the radius $R_1$ of the fringes. The parameters are $\theta_S$=75°, $\theta_H$=75°, S=66.5 cm, H=45 cm, $D_x$=0, and $D_y$=0.

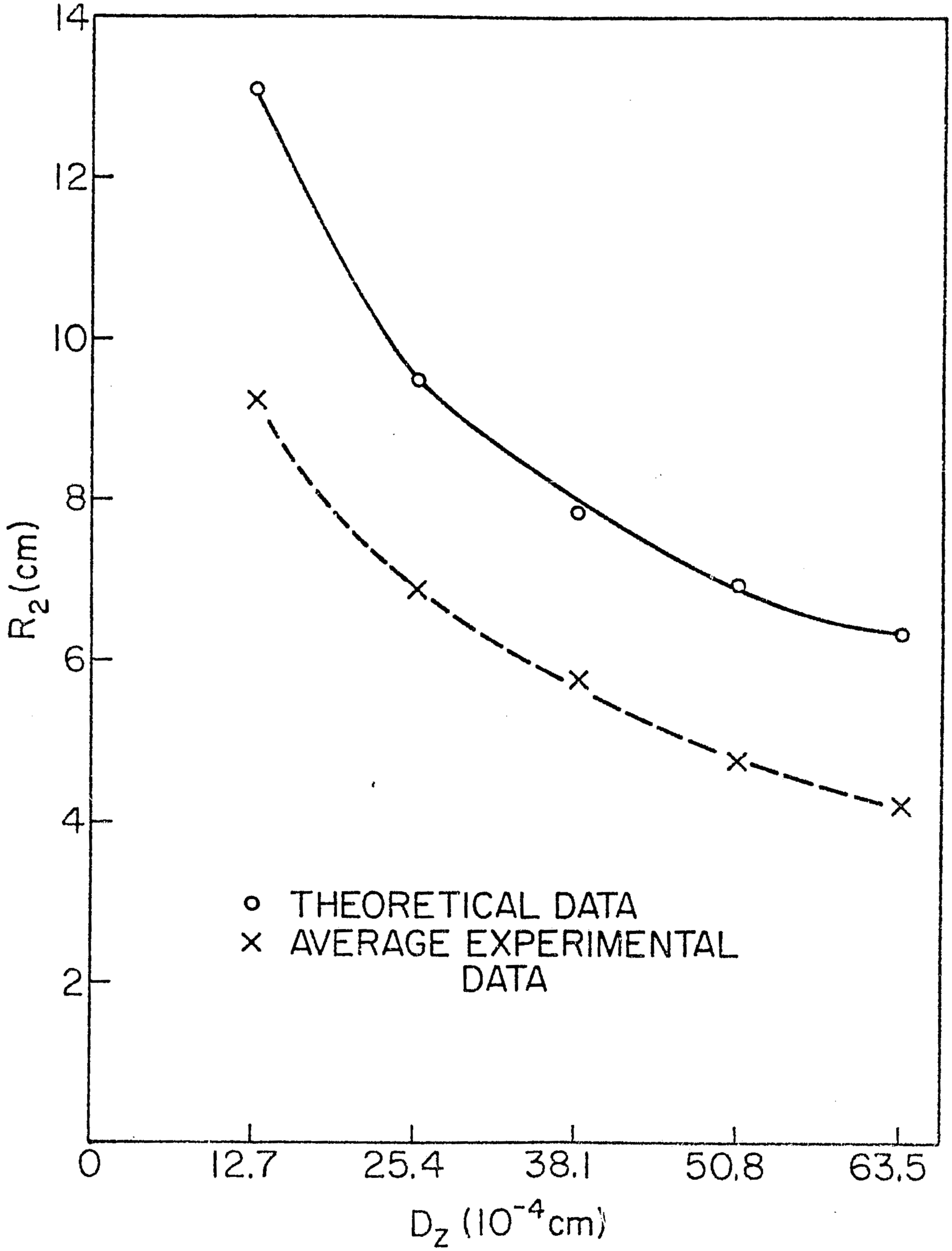


Figure 15 Comparison between theory and experiment for $R_2$. The parameters are $\theta_S$=75°, $\theta_H$=75°, S=66.5 cm, H=45 cm, $D_x$=0, and $D_y$=0.

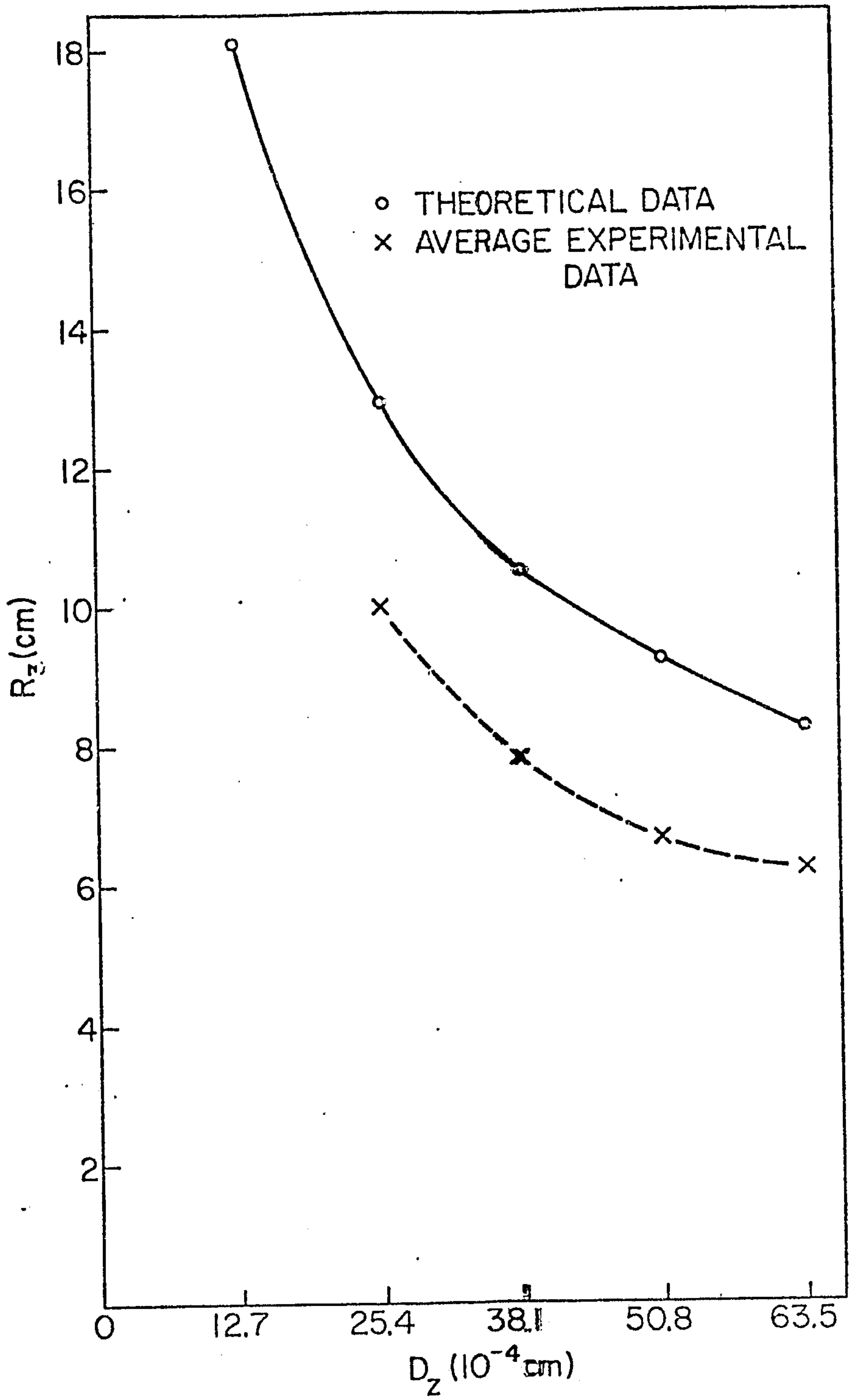


Figure 16 Comparison between theory and experiment for $R_3$. The parameters are $\theta_S$=75°, $\theta_H$=75°, S=66.5 cm, H=45 cm, $D_x$=0, and $D_y$=0.

Table VI. Comparison between theory and experiment for the radii of the fringe loci of the flat plate for $\theta_S = 60°$, $\theta_H = 75°$, H = 45 cm, S = 66.5 cm, $D_x = 0$, and $D_y = 0$.

$\theta_S = 60°$

| $D_z (10^{-4}$ cm) | $R_n$ (cm) | $R_1$ | $R_2$ | $R_3$ | $R_4$ | $R_5$ |
|---|---|---|---|---|---|---|
| 12.7 | V | 6.5 | | | | |
| | H | 7 | | | | |
| | T | 7.69 | 13.2 | 16.96 | 20.0 | 22.7 |
| 25.4 | V | 5 | 9.5 | 12 | | |
| | H | 6 | 10.0 | 12 | | |
| | T | 5.53 | 9.36 | 12.0 | 14.2 | 16.1 |
| 38.1 | V | | 7.6 | | | |
| | H | | 9.4 | | | |
| | T | 4.6 | 7.7 | 9.86 | 1.16 | 1.32 |
| 50.8 | V | 4 | 6 | 7.5 | | |
| | H | 5 | 8.50 | 10 | | |
| | T | 4.04 | 6.7 | 8.6 | 10.1 | 11.4 |
| 63.5 | V | 3.8 | 5.8 | 7 | 8.6 | |
| | H | 5 | 7 | 9 | 10 | |
| | T | 3.7 | 6.0 | 7,7 | 9.1 | 10.0 |

V: Vertical (Exp.)

H: Horizontal (Exp.)

T: Theoretical

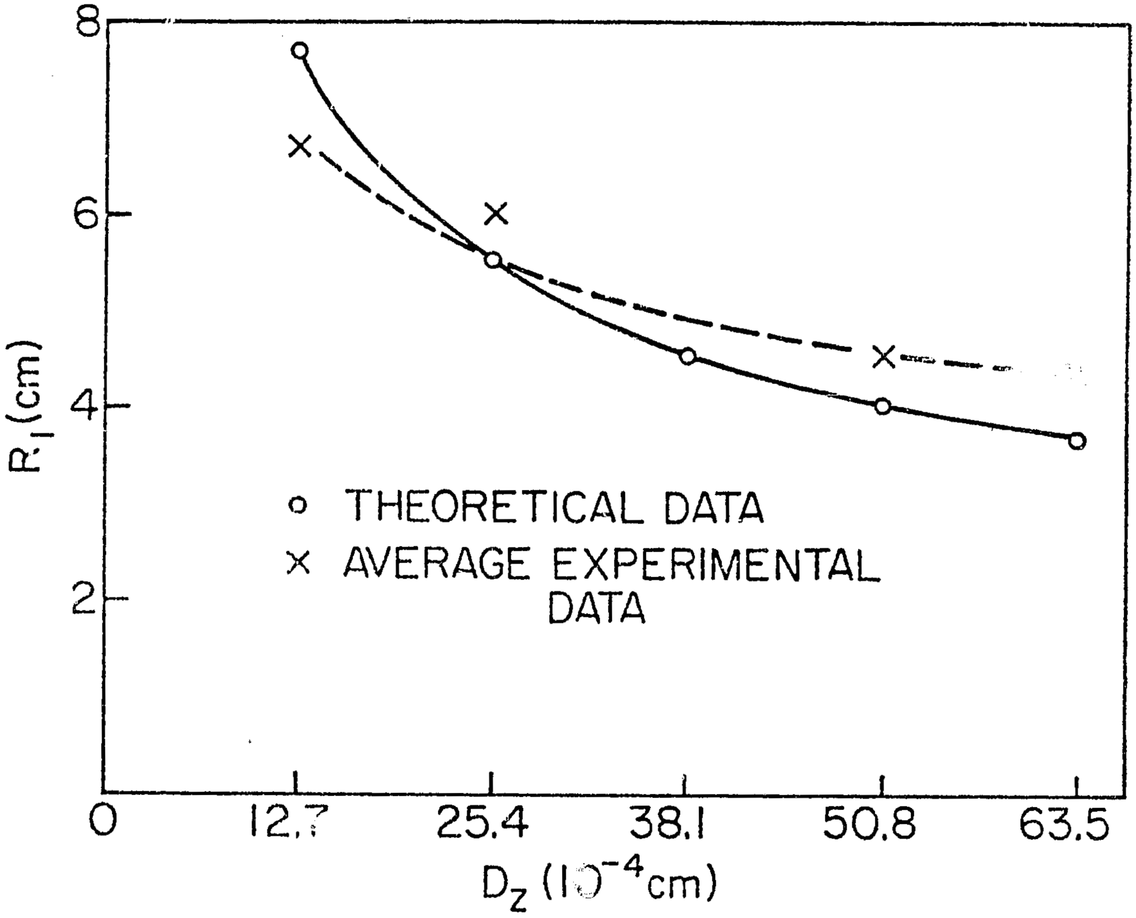


Figure 17 Comparison between theory and experiment for $R_1$, where $\theta_S$=60°, $\theta_H$=75°, S=66.5 cm, H=45 cm, $D_x$=0, and $D_y$=0.

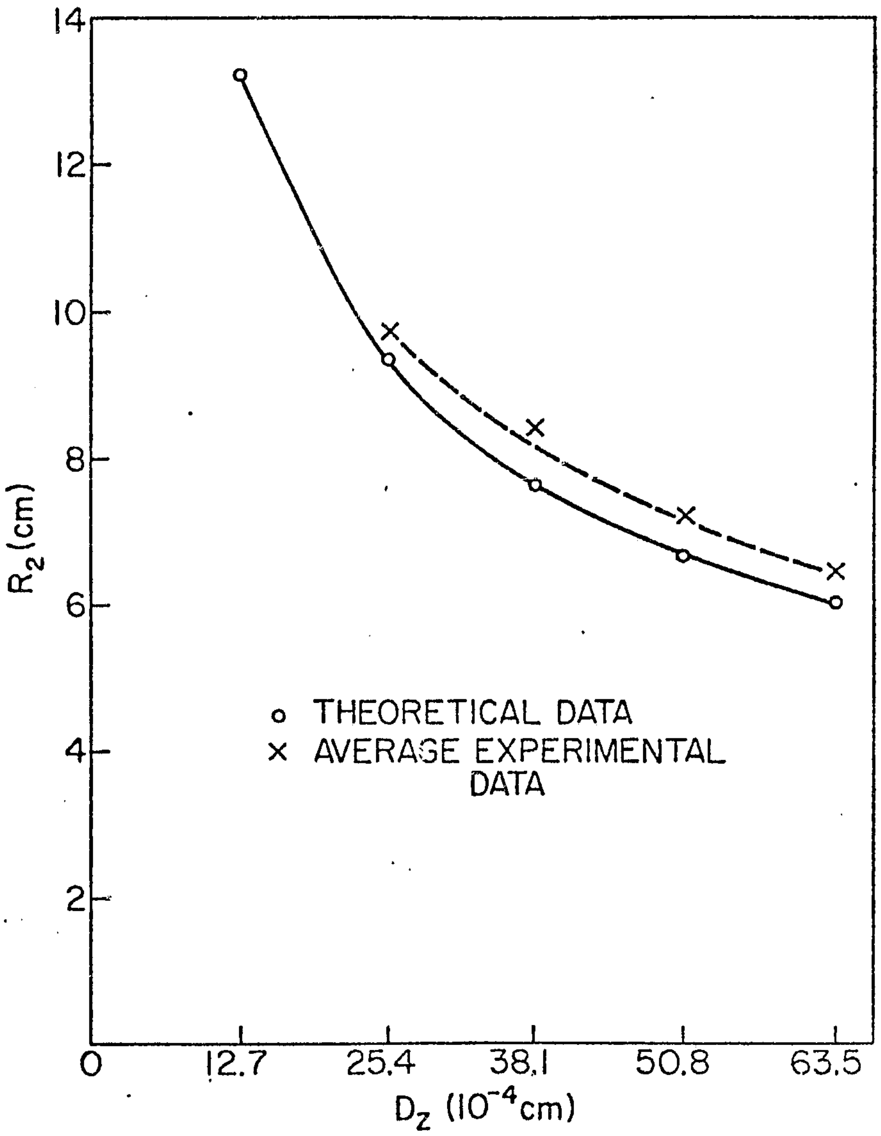


Figure 18 Comparison between theory and experiment for $R_2$, where $\theta_S$=60°, $\theta_H$=75°, S=66.5 cm, H=45 cm, $D_x$=0, and $D_y$=0.

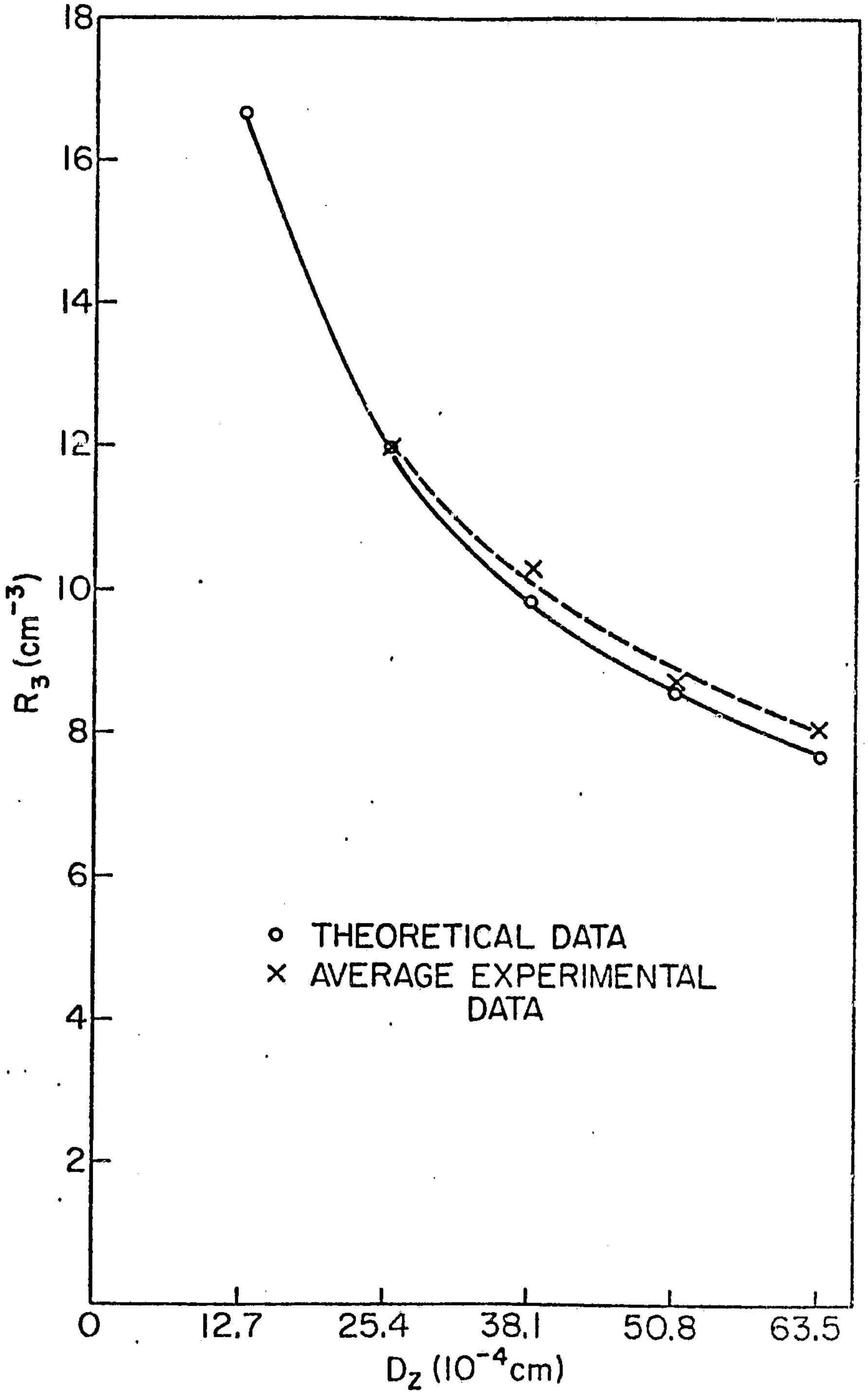


Figure 19 Comparison between theory and experiment for $R_3$, where $\theta_S$=60°, $\theta_H$=75°, S=66.5 cm, H=45 cm, $D_x$=0, and $D_y$=0.

Table VII. Comparison between theory and experiment for the radii of the fringe loci of the flat plate for $\theta_S = 45°$, $\theta_H = 75°$, H = 45 cm, S = 66.5 cm, $D_x = 0$, and $D_y = 0$.

$\theta_S = 45°$

| $D_z$ ($10^{-4}$cm) | $R_n$ | $R_1$ | $R_2$ | $R_3$ | $R_4$ | $R_5$ |
|---|---|---|---|---|---|---|
| 12.7 | V | | | | | |
| | H | | | | | |
| | T | 8.36 | 13.6 | 1.76 | 20.8 | 23.5 |
| 25.4 | V | 7.0 | | | | |
| | H | 7.4 | | | | |
| | T | 6.30 | 10.0 | 12.7 | 14.8 | 16.8 |
| 38.1 | V | 6.0 | 8.0 | | | |
| | H | 7.2 | 9.6 | | | |
| | T | 5.44 | 8.36 | 10.5 | 12.3 | 13.8 |
| 50.8 | V | | | | | |
| | H | | | | | |
| | T | 4.96 | 7.40 | 9.22 | 10.7 | 12.0 |
| 63.5 | V | 4.2 | 6.4 | 8.4 | | |
| | H | 5.8 | 8.0 | 12 | | |
| | T | 4.64 | 6.76 | 8.36 | 9.70 | 10.9 |

V: Vertical (Expt.)

H: Horizontal (Expt.)

T: Theoretical

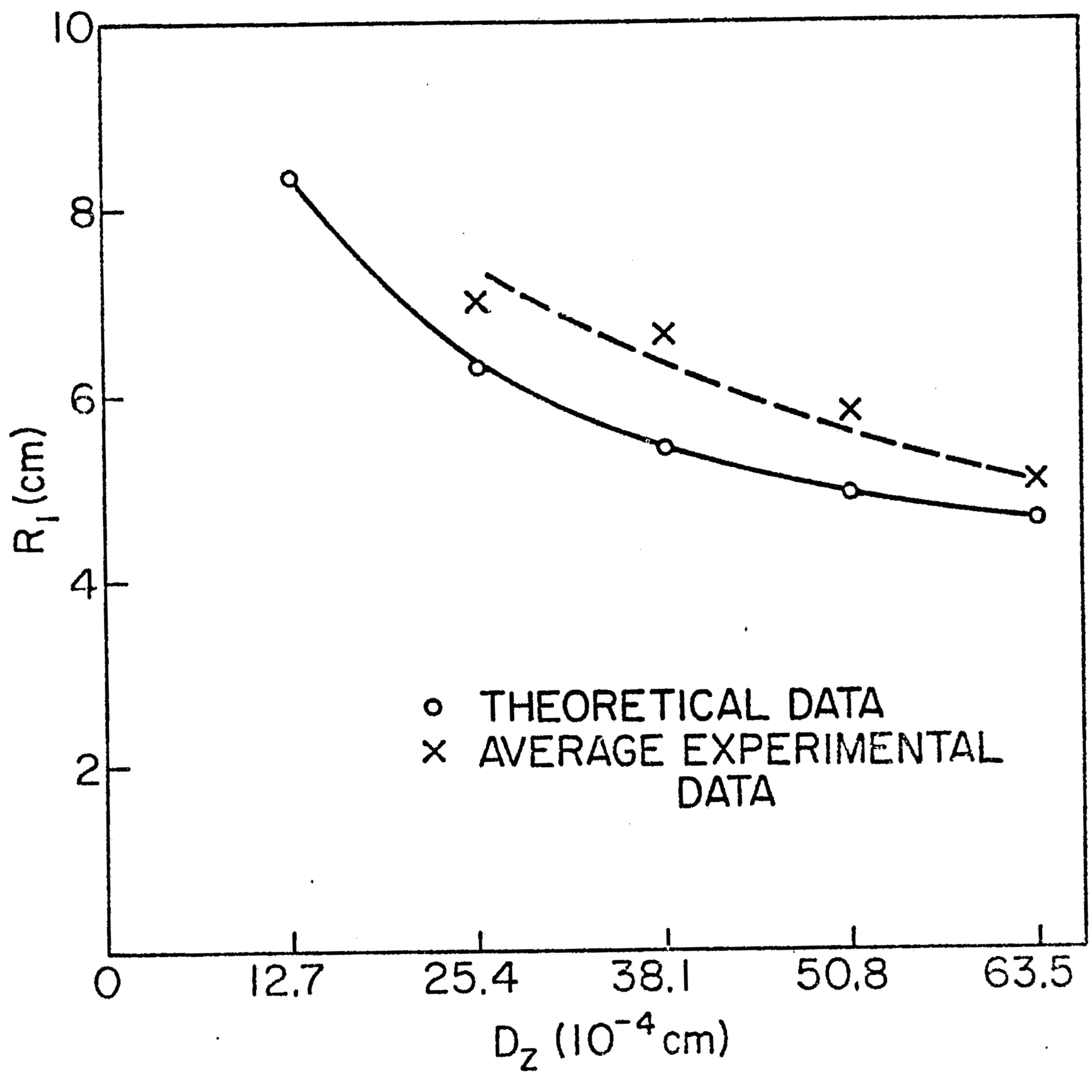


Figure 20. Comparison between theory and experiment for $R_1$, where $\theta_S=45°$, $\theta_H=75°$, S=66.5 cm, H=45 cm, $D_x=0$, and $D_y=0$.

Table VIII. Comparison between theory and experiment for the radii of the fringe loci of the flat plate for $\theta_S = 30°$, $\theta_H = 75°$, $H = 45$ cm, $S = 66.5$ cm, $D_x = 0$, and $D_y = 0$.

$\theta_S = 30°$

| $D_z(10^{-4}$cm) | $R_n$(cm) | $R_1$ | $R_2$ | $R_3$ | $R_4$ | $R_5$ |
|---|---|---|---|---|---|---|
| 12.7 | V | 7 | 11 | | | |
| | H | 8 | 12 | | | |
| | T | 8.23 | 14.1 | 18.1 | 21.4 | 24.3 |
| 25.4 | V | 4.6 | 7 | 9 | | |
| | H | 7. | 9 | 11 | | |
| | T | 5.93 | 10.0 | 12.9 | 15.2 | 17.2 |
| 38.1 | V | 3.6 | 5.4 | 7 | 8 | 9.8 |
| | H | 4.6 | 7 | 8.6 | | |
| | T | 4.93 | 8.23 | 10.5 | 12.4 | 14.1 |
| 50.8 | V | 3 | 4.6 | 5.8 | 6.8 | |
| | H | 4 | 6 | 7.6 | | |
| | T | 4.35 | 7.17 | 9.17 | 10.8 | 12.2 |
| 63.5 | V | 2.6 | 4.2 | 5.4 | 6.2 | 7.2 |
| | H | 4 | 5.8 | 6.8 | 7.8 | |
| | T | 3.96 | 6.46 | 8.23 | 9.68 | 10.9 |

V: Vertical (Expt.)

H: Horizontal (Expt.)

T: Theoretical

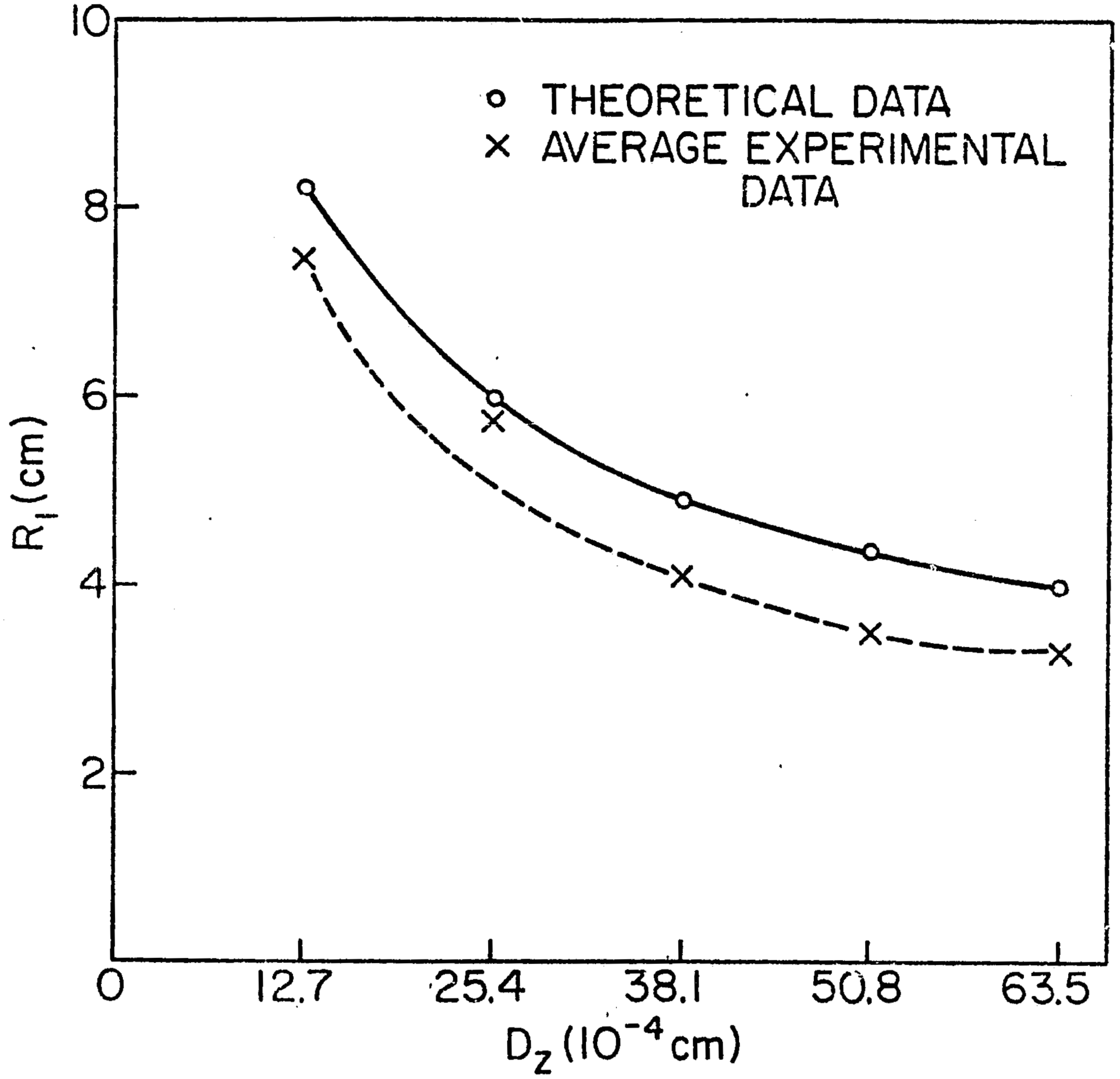


Figure 21 Comparison between theory and experiment for $R_1$, where $\theta_S$=30°, $\theta_H$=75°, S=66.5 cm, H=45 cm, $D_x$=0, and $D_y$=0.

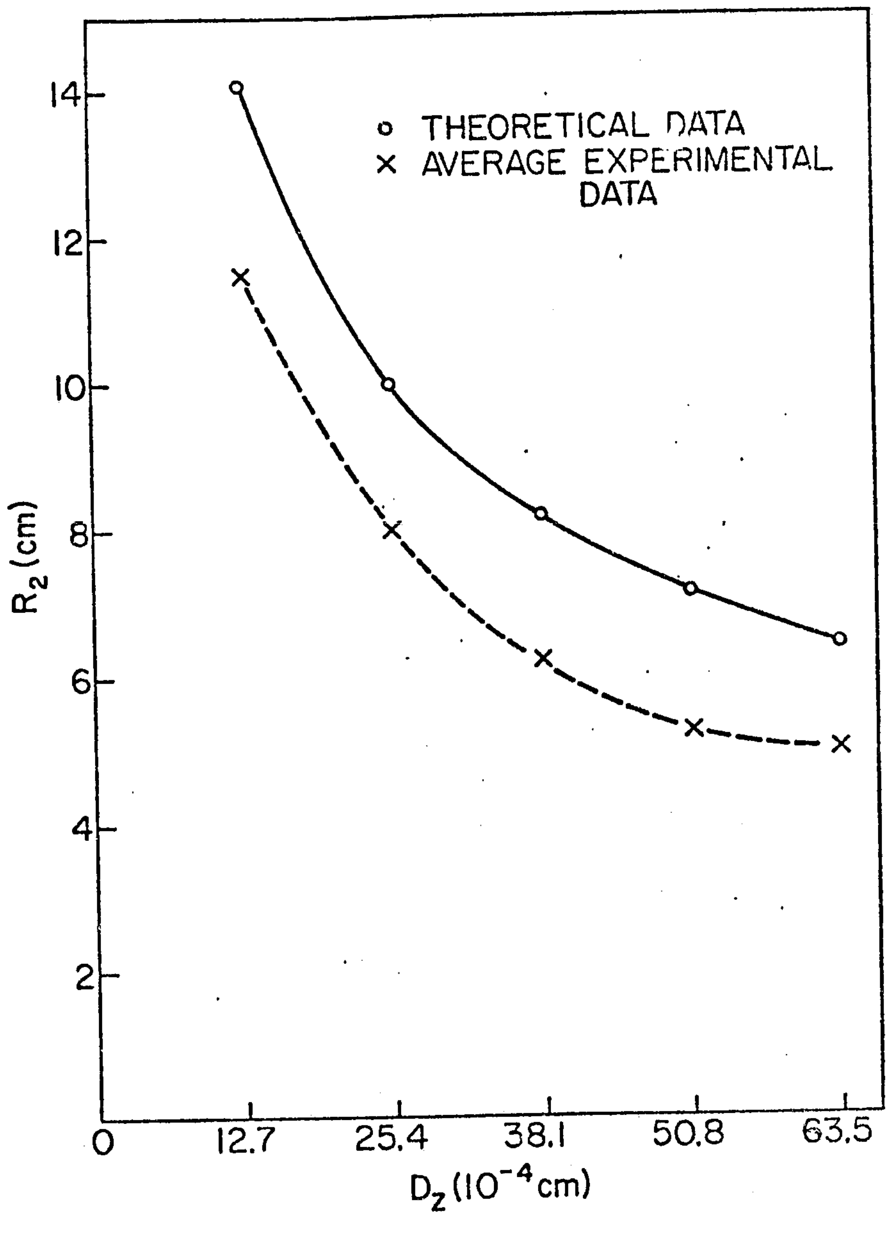


Figure 22 Comparison between theory and experiment for $R_2$, where $\theta_S$=30°, $\theta_H$=75°, S=66.5 cm, H=45 cm, $D_x$=0, and $D_y$=0.

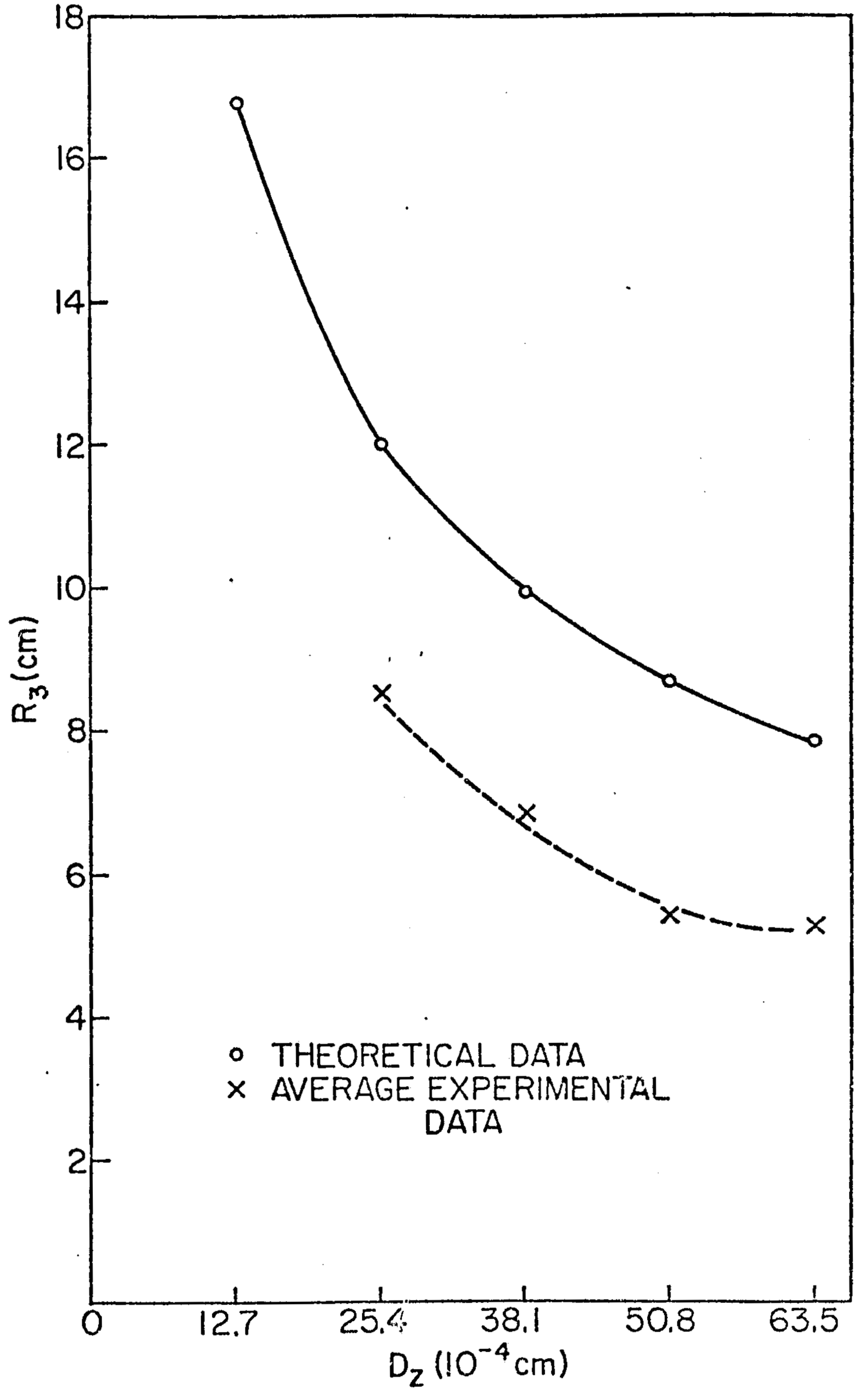


Figure 23 Comparison between theory and experiment for $R_3$, where $\theta_S$=30°, $\theta_H$=75°, S=66.5 cm, H=45 cm, $D_x$=0, and $D_y$=0.

of the radius. This phenomenon showed that: (1) the approximate models are still reasonably satisfactory for curve plates if the angle $90° \geq \theta_S \geq 75°$ in the present system is being selected and, (2) if a curve plate or an object with a curve surface such as that of a main space shuttle engine is being tested, the angle should be cautiously chosen to be greater than or equal to 75° when $\theta_H = 75°$. In other words, it is clear that when both $\theta_S = \theta_H << 75°$, the system is not very appropriate for the test of objects with curve surfaces with regard to the evaluation of the data because light is quite non-uniformly reflected from the surface of these objects to the hologram. This is because the curve surfaces of the objects will unavoidably make non-uniform and reflections which are not accountable by the present theoretical model.

## V. CONCLUSIONS AND SUGGESTIONS

A detailed and quantitative evaluation of the CMHNDT system has been performed according to the tasks specified in the NASA contract NAS8-30479 between the Marshall Space Flight Center and the University of Alabama. The work includes the theoretical interpretation of the double-exposure holographic interference fringe formation due to three-dimensional translations and rotations for this particular system. A simplified model has been derived, and corresponding experimental design and test of the simplified model has been carried out. It is found that under certain realistic conditions, the following theoretical predictions can be made.

(1) For simple motions along a certain axis, in the plane of a flat test object, the fringes are perpendicular to that axis, as viewed through the hologram. with fringe spacing inversely proportional to the amount of displacements.

(2) For displacements normal to the plane of the test object, the fringe loci are concentric circles with centers determined by the system configuration; for large z-component displacement, the high-order fringes are similar to those of a Fresnel-zone plate.

(3) For a combined in-plane and out-of-plane displacement, the fringe loci are also concentric circles and the center of these circular fringes will move along the x-direction, influenced significantly by the x-component of the displacement, and along the y-direction, influenced greatly by the y-component of the displacement, where x and y are the Cartesian coordinates in the plane of the test plate.

(4) Rotations of the surface of the test plate can be treated as equivalent translations and the formula for the translation-type displacement

may be applied.

Experiments have been performed to test the validity of the findings on the simple micrometer-controlled 3-D displacement including in-plane, out-of-plane, and slanted translations, which are quite accurately checked by Michelson interferometers.

In addition, the effect of the incident angle ($\theta_S$) variations as well as the variations of the curvatures of the test plate have also been studied. It may be concluded from the observations of the results that for the system configuration employed, it is better, or even a must, to choose the incident angle as close to 90° (perpendicular to the object) as possible, especially when objects with curved front surfaces with large curvatures are being tested.

The comparisons between the theory and the experiment have shown satisfactory agreements, except for a few minor discrepancies, which can be logically explained. It is extremely difficult to locate the true theoretical center of the circular loci as well as the real values of the radii with respect to the theoretical predictions. However, since the discrepancies are generally small, which suggest that in the application of the system in the real testing environment, for the sake of a more accurate assessment of the displacement from the fringe loci, a calibration plate should be included in the CMHNDT system. The calibration system can simply be the flat test plate and the translation stage used in this study. It may be placed in a convenient position close to but separated from the object being tested. For every double-exposure hologram, the calibration plate will make independent and accurately controlled displacement while the object under test is undergoing a specific loading process. When the data from the hologram are taken, a comparison between theory and experiment with calibration can be made to determine the displacement due to the flaws in the object being tested.

Finally it is suggested that the newly advanced techniques of speckle holography and photography be studied, and the feasibility of the incorporation of these techniques into the already well-studied CMHNDT system be explored. The advantage of this work is to enhance the stability of the system, reduce the stringent equipment requirement, and therefore make the CMHNDT system more flexible in a real testing environment.

## Appendix A

### Derivation of Eq. (25)

$$\delta(\Delta L_2) \equiv (\Delta L_2)_{\text{at }(x,y)} - (\Delta L_2)_{\text{at }(0,0)}$$

$$= \frac{-1}{S^3}\{\frac{1}{2}[2(\vec{t}\cdot\vec{S}) - (\vec{D}\cdot\vec{t}) - t^2] \times [(\vec{D}\cdot\vec{S}) - (\vec{D}\cdot\vec{t}) - \frac{D^2}{2}]$$

$$+ \frac{1}{2}[(\vec{D}\cdot\vec{S}) - \frac{D^2}{2}][-(\vec{D}\cdot\vec{t})]\}$$

$$\frac{-1}{H^3}\{\frac{1}{2}[2(\vec{t}\cdot\vec{H}) - (\vec{D}\cdot\vec{t}) - t^2] \times [(\vec{D}\cdot\vec{H}) - (\vec{D}\cdot\vec{t}) - \frac{D^2}{2}]$$

$$+ \frac{1}{2}[(\vec{D}\cdot\vec{H}) - \frac{D^2}{2}][-(\vec{D}\cdot\vec{t})]\}$$

$$= \frac{-1}{S^3}\{(\vec{t}\cdot\vec{S})(\vec{D}\cdot\vec{S}) - (\vec{t}\cdot\vec{S})[(\vec{D}\cdot\vec{t}) + \frac{D^2}{2}] - (\vec{D}\cdot\vec{t})[(\vec{D}\cdot\vec{S}) - \frac{D^2}{2}]$$

$$+ \frac{1}{2}(\vec{D}\cdot\vec{t})^2 - \frac{1}{2}t^2[(\vec{D}\cdot\vec{S}) - (\vec{D}\cdot\vec{t}) - \frac{D^2}{2}]\}$$

$$- \frac{1}{H^3}\{(\vec{t}\cdot\vec{H})(\vec{D}\cdot\vec{H}) - (\vec{t}\cdot\vec{H})[(\vec{D}\cdot\vec{t}) + \frac{D^2}{2}] - (\vec{D}\cdot\vec{t})](\vec{D}\cdot\vec{H}) - \frac{D^2}{2}]$$

$$+ \frac{1}{2}(\vec{D}\cdot\vec{t})^2 - \frac{1}{2}t^2[(\vec{D}\cdot\vec{H}) - (\vec{D}\cdot\vec{t}) - \frac{D^2}{2}]\}$$

$$= -\frac{1}{S^3}(\vec{t}\cdot\vec{S})(\vec{D}\cdot\vec{S}) - \frac{1}{H^3}(\vec{t}\cdot\vec{H})(\vec{D}\cdot\vec{H}) + [\vec{t}\cdot(\frac{\vec{S}}{S^3} + \frac{\vec{H}}{H^3})][(\vec{D}\cdot\vec{t}) + \frac{D^2}{2}]$$

$$+ (\vec{D}\cdot\vec{t})[\vec{D}\cdot(\frac{\vec{S}}{S^3} + \frac{\vec{H}}{H^3}) - (\frac{1}{S^3} + \frac{1}{H^3})\frac{D^2}{2}] - \frac{1}{2}[\frac{1}{S^3} + \frac{1}{H^3}](\vec{D}\cdot\vec{t})^2$$

$$+ \frac{1}{2}t^2[\vec{D}\cdot(\frac{\vec{S}}{S^3} + \frac{\vec{H}}{H^3}) - (\frac{1}{S^3} + \frac{1}{H^3})(\vec{D}\cdot\vec{t}) - \frac{1}{2}(\frac{1}{S^3} + \frac{1}{H^3})D^2]$$

$$= -\frac{1}{2}\left(\frac{1}{S^3}+\frac{1}{H^3}\right)(\vec{D}\cdot\vec{t})t^2 + \left\{\frac{1}{2}\left[\vec{D}\cdot\left(\frac{\vec{S}}{S^3}+\frac{\vec{H}}{H^3}\right) - \frac{1}{2}\left(\frac{1}{S^3}+\frac{1}{H^3}\right)D^2\right]t^2\right.$$

$$-\frac{1}{2}\left(\frac{1}{S^3}+\frac{1}{H^3}\right)(\vec{D}\cdot\vec{t})^2 + \left.\left[\left(\frac{\vec{S}}{S^3}+\frac{\vec{H}}{H^3}\right)\cdot\vec{t}\right](\vec{D}\cdot\vec{t})\right\}$$

$$-\left\{\left[\left(\frac{1}{S^3}+\frac{1}{H^3}\right)\frac{D^2}{2} - \vec{D}\cdot\left(\frac{\vec{S}}{S^3}+\frac{\vec{H}}{H^3}\right)\right](\vec{D}\cdot\vec{t}) - \frac{D^2}{2}\left(\frac{\vec{S}}{S^3}+\frac{\vec{H}}{H^3}\right)\cdot\vec{t}\right.$$

$$\left.+\frac{1}{S^3}(\vec{S}\cdot\vec{D})(\vec{S}\cdot\vec{t}) + \frac{1}{H^3}(\vec{H}\cdot\vec{D})(\vec{H}\cdot\vec{t})\right\} \quad . \qquad (25)$$

# Appendix B

## Second-Order Contribution of $D_x$ to $\delta(\Delta L_2)$

If $D = D_x \hat{i}$, then Eq. (25) becomes

$$\delta(\Delta L_2) = \{-\frac{1}{2}(\frac{1}{S^3} + \frac{1}{H^3})(D_x x)(x^2 + y^2)\}$$

$$+ \{[\frac{1}{2} D_x(\frac{-\cos\theta_S}{S^2} + \frac{\cos\theta_H}{H^2}) - \frac{1}{2}(\frac{1}{S^3} + \frac{1}{H^3}) D_x^2](x^2 + y^2)$$

$$- \frac{1}{2}(\frac{1}{S^3} + \frac{1}{H^3}) D_x^2 x^2 + (\frac{-\cos\theta_S}{S^2} + \frac{\cos\theta_H}{H^2}) D_x x^2\}$$

$$- \{[D_x^2 - D_x(\frac{-\cos\theta_S}{S^2} + \frac{\cos\theta_H}{H^2})] D_x x$$

$$- \frac{D_x^2}{2}(\frac{-\cos\theta_S}{S^2} + \frac{\cos\theta_H}{H^2}) x$$

$$+ \frac{1}{S}(D_x \cos^2\theta_S)x + \frac{1}{H}(D_x \cos^2\theta_H)x\}$$

$$= \{-\frac{1}{2}(\frac{1}{S^3} + \frac{1}{H^3}) D_x(x^2 + y^2)x$$

$$+ \{[\frac{3}{2} D_x(\frac{-\cos\theta_S}{S^2} + \frac{\cos\theta_H}{H^2}) - (\frac{1}{S^3} + \frac{1}{H^3})D_x^2]x^2$$

$$+ [\frac{1}{2} D_x(\frac{-\cos\theta_S}{S^2} + \frac{\cos\theta_H}{H^2}) - \frac{1}{2}(\frac{1}{S^3} + \frac{1}{H^3})D_x^2]y^2\}$$

$$- \{D_x^2[1 + \frac{3}{2}(\frac{\cos\theta_S}{S^2} - \frac{\cos\theta_H}{H^2})] + D_x(\frac{\cos^2\theta_S}{S} + \frac{\cos^2\theta_H}{H})\}x \quad .$$

# Appendix C

## Second-Order Contribution of $D_y$ to $\delta(\Delta L_2)$

If $D = D_y\,\hat{j}$, then Eq. (25) becomes

$$\delta(\Delta L_2) = -\frac{1}{2}\left(\frac{1}{S^3} + \frac{1}{H^3}\right)(D_y y)(x^2 + y^2)$$

$$+ \left\{\frac{-D_y^{\,2}}{2}\left(\frac{1}{S^3} + \frac{1}{H^3}\right)(x^2 + y^2) - \frac{1}{2}\left(\frac{1}{S^3} + \frac{1}{H^3}\right)D_y^{\,2}y^2 + \left(\frac{-x\cos\theta_S}{S^2} + \frac{x\cos\theta_H}{H^2}\right)D_y y\right\}$$

$$+ \left\{\frac{D_y^{\,2}}{2}\left(\frac{-\cos\theta_S}{S^2} + \frac{\cos\theta_H}{H^2}\right)x\right\}$$

$$= -\frac{1}{2}\left(\frac{1}{S^3} + \frac{1}{H^3}\right)D_y(x^2 + y^2)y$$

$$- \left[\frac{D_y^{\,2}}{2}\left(\frac{1}{S^3} + \frac{1}{H^3}\right)x^2 + D_y^{\,2}\left(\frac{1}{S^3} + \frac{1}{H^3}\right)y^2 + D_y\left(\frac{\cos\theta_S}{S^2} - \frac{\cos\theta_H}{H^2}\right)xy\right]$$

$$+ \frac{D_y^{\,2}}{2}\left(\frac{-\cos\theta_S}{S^2} + \frac{\cos\theta_H}{H^2}\right)x \quad .$$

# Appendix D

## The Computer Program

This computer program is designed for the computation of the fringe loci based on the simple model as given by Eq. (59), (60) and (61) in the main text of the report. Output shows the fringe spacing, center's location and radii of the fringes.

```
@FOR,IS MAIN
FOR 0E2B-02/10/76-13:54:02 (,0)

   MAIN PROGRAM

   STORAGE USED: CODE(1) 000527; DATA(0) 000607; BLANK COMMON(2) 000000


   EXTERNAL REFERENCES (BLOCK, NAME)

    0003    NINTR$
    0004    NRDU$
    0005    NIO2$
    0006    NWDU$
    0007    NIO1$
    0010    SIN
    0011    SQRT
    0012    NSTOP$


   STORAGE ASSIGNMENT  (BLOCK, TYPE, RELATIVE LOCATION, NAME)

    0001     000134 1L         0001     000457 100L        0001     000517 1000L       0001     000040 121G        0001     000053 130G
    0001     000066 137G       0001     000477 150L        0001     000314 223G        0001     000074 5L          0001     000421 50L
    0001     000363 500L       0000     000451 800F        0000     000422 810F        0000     000453 825F        0000     000511 900F
    0000     000520 905F       0000     000470 910F        0000     000526 915F        0000     000533 918F        0000     000543 920F
    0000     000553 925F       0000     000437 930F        0000     000410 935F        0000     000425 940F        0000     000454 977F
    0000 R 000376 A            0000 R 000403 ADX          0000 R 000404 ADY          0000 R 000374 ADZ          0000 R 000375 B
    0000 R 000377              0000 R 000407 DELTA        0000 R 000405 DELTX        0000 R 000406 DELTY        0000 R 000370 DX
    0000 R 000131 DX1          0000 R 000371 DY           0000 R 000213 DY1          0000 R 000372 DZ           0000 R 000275 DZ1
    0000 R 000402 F            0000 R 000373 FACT         0000 R 000366 H            0000 R 000035 H1           0000 I 000362 I
    0000 I 000361 K            0000 R 000000 LAMD         0000 I 000367 N            0000 I 000360 NA           0000 I 000357 ND
    0000 R 000001 R            0000 R 000365 S            0000 R 000011 S1           0000 R 000363 THETAH       0000 R 000364 THETAS
    0000 R 000061 THETA1       0000 R 000105 THETA2       0000 R 000400 XC           0000 R 000401 YC


00101      1*              REAL LAMD                                                         000000
00103      2*              DIMENSION R(8),S1(20),H1(20),THETA1(20),THETA2(20)                000001
00104      3*              DIMENSION DX1(50),DY1(50),DZ1(50)                                 000001
00105      4*              READ(5,825) ND                                                    000001
00110      5*              READ(5,825) NA                                                    000007
00110      6*        C     ND=NUMBER OF DATA SETS(TRANSLATIONS)TO BE READ IN                 000007
00110      7*        C      NA=NUMBER OF ANGELS ON OBJECT BEAM TO BE READ IN                 000007
00113      8*              K=0                                                               000015
00114      9*              WRITE(6,935)                                                      000022
00116     10*          935 FORMAT(/////,15X,'ALL DIST. IN CM. ,ALL ANGLES IN DEGREES')       000031
00117     11*              READ(5,810) (H1(I),THETA1(I),I=1,NA)                              000031
00126     12*              READ(5,810) (S1(I),THETA2(I),I=1,NA)                              000044
00135     13*              READ(5,800) (DX1(I),DY1(I),DZ1(I),I=1,ND)                         000057
00145     14*          810 FORMAT(F10.5,F10.5)                                               000074
00146     15*          5   K=K+1                                                             000074
00147     16*              WRITE(6,940) H1(K),THETA1(K)                                      000076
00153     17*          940 FORMAT(/////,15X,'H',5X,1PE15.6,//,15X,'THETA H',5X,1PE15.6)      000107
00154     18*              WRITE(6,930) S1(K),THETA2(K)                                      000107
00156     19*          930 FORMAT(////,15X,'S',5X,1PE15.6,//,15X,'THETA S',5X,1PE15.6)       000116
```

```
      THETAH = THETA1(K)*3.141592654/180.
      THETAS = THETA2(K)*3.141592654/180.
      S = S1(K)
      H= H1(K)
      N = 0
    1 CONTINUE
      N = N+1
      IF(N.GT.ND) GO TO 1000
      DX = DX1(N)
      DY = DY1(N)
      DZ = DZ1(N)
  800 FORMAT(3F10.4)
      FACT = 1.E-4.
      DX=DX*FACT
      DY = DY*FACT
      DZ = DZ*FACT
  825 FORMAT(I3)
      WRITE(6,977) DX,DY,DZ
  977 FORMAT(///,15X,'DX=',1PE15.6,//,15X,'DY=',1PE15.6,
     1  //,15X,'DZ=', 1PE15.6)
      LAMD = 4.880E-5
      ADZ = ABS(DZ)
      IF(ADZ.LT.1.0E-8) GO TO 500
      A=.5*DZ*(SIN(THETAS)/(S**2.) + SIN(THETAH)/(H**2.))
      B=DZ*(SIN(2.*THETAS)/(2.*S) - SIN(2.*THETAH)/(2.*H))
     1  + DX*(1./S + 1./H)
      C= DY*(1./S +1./H)
      XC= -B/(2.*A)
      YC=-C/(2.*A)
      DO 25 I=1,4
      F=I
      R(I) = (1./(2.*A))*SQRT(B**2.+C**2.+4.*A*(F-.5)*LAMD)
   25 CONTINUE
      WRITE(6,900)  XC,YC
      WRITE(6,905)
      WRITE(6,910) R(1),R(2),R(3),R(4)
  910  FORMAT(//,15X,'R(1)=',1PE15.8,/,15X,'R(2)=',1PE15.8,
     1/,15X,'R(3)=',1PE15.8,/,15X,'R(4)=',1PE15.8)
  900 FORMAT(///,15X,'XC=',1PE15.8,'YC=',1PE15.8)
  905 FORMAT(//,15X,'RADII OF CIRC. FRINGES')
      GO TO 1
  500 ADX=ABS(DX)
      ADY = ABS(DY)
      IF((ADX.GT.1.E-10).AND.(ADY.GT.1E-10))  GO TO 50
      IF(ADX.GT.1.E-10) GO TO 100
      IF(ADY.GT.1.E-10) GO TO 150
      WRITE(6,915)
  915 FORMAT(///,15X,'NO TRANSLATION')
      GO TO 1
   50 DELTX=LAMD/(DX*(1./S+1./H))
      DELTY=LAMD/(DY*(1./S+1./H))
      DELTA=SQRT(DELTX**2. +DELTY**2.)
      WRITE(6,918) DELTA
  918 FORMAT(///,15X,'SLANT FRINGE SPACING IS',1PE15.8)
      GO TO 1
  100 DELTX=LAMD/(DX*(1./S+1./H))
      WRITE(6,920) DELTX
```

```
00301     77*      920 FORMAT(///,15X,'VERTICAL FRINGE SPACING IS',1PE15.8)          000475
00302     78*          GO TO 1                                                       000475
00303     79*      150 DELTY=LAMD/(DY*(1./S+1./H))                                   000477
00304     80*          WRITE(6,925) DELTY                                            000507
00307     81*      925 FORMAT(///,15X,'HORIZONTAL FRINGE SPACING IS',1PE15.8)        000515
00310     82*          GO TO 1                                                       000515
00311     83*     1000 IF(K.LT.NA) GO TO 5                                           000517
00313     84*          STOP                                                          000522
00314     85*          END                                                           000526

     END OF COMPILATION:        NO  DIAGNOSTICS.


@XQT
RMAP-16-02/10-15:54




ADDRESS LIMITS      001000 011660     040000 044471
STARTING ADDRESS    011132

WORDS DECIMAL        4529 IBANK        2362 DBANK


NSWTC$/FOR69              1   001000 001024
NBACK$/FOR-E2             1   001025 001047
NRWND$/FOR-E2             1   001050 001133      2   040000 040011
NREW$/FOR-E2              1   001134 001341      2   040012 040031
NBDCV$/FOR64              1   001342 001467      2   040032 040074
NFTCH$/FOR-E2             1   001470 001752      2   040075 040110
NFTV$/FOR-E2              1   001753 001775
NCNT$/FOR68               1   001776 002217      2   040111 040205
NCLOS$/FOR-E2             1   002220 002452      2   040206 040233
NBLK$/FOR68               1   002453 002564
NBSEL$/FOR68              1   002565 002625
NOPEN$/FOR68              1   002626 002661
NSFOB$/FOR-E2                                    2   040234 042435
NOTINT/FOR68              1   002662 003156      2   042436 042441
NOOTS/FOR-E2C             1   003157 004333      2   042442 042500
NIOER$/FOR-E2             1   004334 004525      2   042501 042646
NINTR$/FOR68              1   004526 004716      2   042647 042652
NINTS/FOR-E2C             1   004717 006070      2   042653 042707
NFMT$/FOR-E2C             1   006071 006753      2   042710 042764
NFORM$/FOR69              1   006754 007741      2   042765 043140
                                                 4   043141 043212
NTAB$/FOR-E2                                     2   043213 043251
ERR1/SYS70-6
```

```
NERR$/FOR-E2          1   007742 010365      2   043252 043456
NSTOP$/FOR69          1   010366 010412      2   043457 043466
SQRT$/FOR69           1   010413 010453      2   043467 043500
SINCOS$/FOR69         1   010454 010606      2   043501 043522
MODUF$/FOR6:          1   010607 010647
NIONS/FOR-E2          1   010650 011026      2   043523 043641
NIDUF$/FOR-E2         1   011027 011066      2   043642 043642
NINTRS/FOR-E2A        1   011067 011131      2   043643 043662
BLANK$COMMON (COMMON BLOCK)
MAIN                  1   011132 011660      0   043663 044471
                                             2   BLANK$COMMON

SYS$*RLIB$. LEVEL 70-6
END RMAP: 1.486 SECONDS, 031 BLOCKS.
```

ALL DIST. IN CM. ,ALL ANGLES IN DEGREES

H 4.500000+01

THETA H 7.500000+01

S 6.650000+01

THETA S 1.500000+01

DX= 5.080000-04

DY= 0.000000

DZ= 2.540000-03

XC= -1.05611975+01YC= 0.00000000

RADII OF CIRC. FRINGES

R(1)= 1.21414559+01
R(2)= 1.48042924+01
R(3)= 1.70563536+01
R(4)= 1.90439312+01

```
DX=     1.016000-03

DY=     0.000000

DZ=     2.540000-03


XC= -2.44763949+01YC=  0.00000000

RADII OF CIRC. FRINGES

R(1)=  2.51986101+01
R(2)=  2.65842450+01
R(3)=  2.79011505+01
R(4)=  2.91586409+01


DX=     1.524000-03

DY=     0.000000

DZ=     2.540000-03


XC= -3.83915920+01YC=  0.00000000

RADII OF CIRC. FRINGES

R(1)=  3.88560209+01
R(2)=  3.97686119+01
R(3)=  4.06607256+01
R(4)=  4.15336619+01


DX=     2.032000-03

DY=     0.000000

DZ=     2.540000-03


XC= -5.23067894+01YC=  0.00000000

RADII OF CIRC. FRINGES

R(1)=  5.26486106+01
R(2)=  5.33256817+01
R(3)=  5.39942632+01
R(4)=  5.40546664+01


DX=     2.540000-03

DY=     0.000000

DZ=     2.540000-03


XC= -6.62219868+01YC=  0.00000000

RADII OF CIRC. FRINGES

R(1)=  6.64923115+01
R(2)=  6.70296917+01
R(3)=  6.75627975+01
R(4)=  6.80917311+01


DX=     5.080000-04

DY=     0.000000

DZ=     5.080000-03


XC= -3.60359889+00YC=  0.00000000

RADII OF CIRC. FRINGES

R(1)=  5.56093115+00
R(2)=  8.17312765+00
R(3)=  1.01329205+01
R(4)=  1.17708173+01


DX=     1.016000-03

DY=     0.000000

DZ=     5.080000-03
```

```
XC= -1.05611975+01YC=  0.00000000

RADII OF CIRC. FRINGES

R(1)=  1.13787926+01
R(2)=  1.26589650+01
R(3)=  1.41855223+01
R(4)=  1.53982177+01

DX=    1.524000-03

DY=    0.000000

DZ=    5.080000-03

XC= -1.75187960+01YC=  0.00000000

RADII OF CIRC. FRINGES

R(1)=  1.80234911+01
R(2)=  1.89926906+01
R(3)=  1.99147775+01
R(4)=  2.07960196+01

DX=    2.032000-03

DY=    0.000000

DZ=    5.080000-03

XC= -2.44763949+01YC=  0.00000000

RADII OF CIRC. FRINGES

R(1)=  2.48401270+01
R(2)=  2.55520642+01
R(3)=  2.62446957+01
R(4)=  2.69195116+01

DX=    2.540000-03

DY=    0.000000

DZ=    5.080000-03

XC= -3.14339936+01YC=  0.00000000

RADII OF CIRC. FRINGES

R(1)=  3.17180381+01
R(2)=  3.22786307+01
R(3)=  3.28296523+01
R(4)=  3.33715768+01

H          4.500000+01

THETA H          7.500000+01

S          6.650000+01

THETA S          3.000000+01

DX=    5.080000-04

DY=    0.000000

DZ=    2.540000-03

XC= -1.42490681+01YC=  0.00000000

RADII OF CIRC. FRINGES

R(1)=  1.53491392+01
R(2)=  1.73411748+01
R(3)=  1.91268561+01
R(4)=  2.07595015+01

DX=    1.016000-03
```

DY= 0.000000

DZ= 2.540000-03

XC= -2.68761223+01YC= 0.00000000

RADII OF CIRC. FRINGES

R(1)= 2.74771466+01
R(2)= 2.86376300+01
R(3)= 2.97528844+01
R(4)= 3.08278189+01

DX= 1.524000-03

DY= 0.000000

DZ= 2.540000-03

XC= -3.95071769+01YC= 0.00000000

RADII OF CIRC. FRINGES

R(1)= 3.99171281+01
R(2)= 4.07246532+01
R(3)= 4.15164747+01
R(4)= 4.22934737+01

DX= 2.032000-03

DY= 0.000000

DZ= 2.540000-03

XC= -5.21362309+01YC= 0.00000000

RADII OF CIRC. FRINGES

R(1)= 5.24475617+01
R(2)= 5.30647435+01
R(3)= 5.36748285+01
R(4)= 5.42780576+01

DX= 2.540000-03

DY= 0.000000

DZ= 2.540000-03

XC= -6.47652855+01YC= 0.00000000

RADII OF CIRC. FRINGES

R(1)= 6.50161695+01
R(2)= 6.55150557+01
R(3)= 6.60101719+01
R(4)= 6.65016022+01

DX= 5.080000-04

DY= 0.000000

DZ= 5.080000-03

XC= -7.93454099+00YC= 0.00000000

RADII OF CIRC. FRINGES

R(1)= 8.90151715+00
R(2)= 1.05734169+01
R(3)= 1.20148777+01
R(4)= 1.33010308+01

DX= 1.016000-03

DY= 0.000000

DZ= 5.080000-03

XC= -1.42490681+01YC= 0.00000000

RADII OF CIRC. FRINGES

```
R(1)=  1.48093218+01
R(2)=  1.56706064+01
R(3)=  1.66652369+01
R(4)=  1.76043931+01


DX=     1.524000-03

DY=     0.000000

DZ=     5.080000-03


XC= -2.05635951+01YC=  0.00000000
```

RADII OF CIRC. FRINGES

```
R(1)=  2.09557033+01
R(2)=  2.17186935+01
R(3)=  2.24557741+01
R(4)=  2.31694179+01


DX=     2.032000-03

DY=     0.000000

DZ=     5.080000-03


XC= -2.66781223+01YC=  0.00000000
```

RADII OF CIRC. FRINGES

```
R(1)=  2.71792846+01
R(2)=  2.77718141+01
R(3)=  2.83519628+01
R(4)=  2.89204760+01


DX=     2.540000-03

DY=     0.000000

DZ=     5.080000-03


XC= -3.31926494+01YC=  0.00000000
```

RADII OF CIRC. FRINGES

```
R(1)=  3.34369860+01
R(2)=  3.39203796+01
R(3)=  3.43969808+01
R(4)=  3.48670683+01


H              4.500000+01

THETA H            7.500000+01


S              6.650000+01

THETA S            4.500000+01


DX=     5.080000-04

DY=     0.000000

DZ=     2.540000-03


XC= -1.47829096+01YC=  0.00000000
```

RADII OF CIRC. FRINGES

```
R(1)=  1.57702351+01
R(2)=  1.75793090+01
R(3)=  1.92188425+01
R(4)=  2.07291028+01


DX=     1.016000-03

DY=     0.000000
```

DZ=     2.540000-03

XC= -2.64833140+01YC=  0.00000000

RADII OF CIRC. FRINGES

R(1)=  2.70468445+01
R(2)=  2.81400712+01
R(3)=  2.91923662+01
R(4)=  3.02080650+01

DX=     1.524000-03

DY=     0.000000

DZ=     2.540000-03

XC= -3.81837182+01YC=  0.00000000

RADII OF CIRC. FRINGES

R(1)=  3.85767055+01
R(2)=  3.93509033+01
R(3)=  4.01101708+01
R(4)=  4.08553252+01

DX=     2.032000-03

DY=     0.000000

DZ=     2.540000-03

XC= -4.96841224+01YC=  ^.00000000

RADII OF CIRC. FRINGES

R(1)=  5.01855712+01
R(2)=  5.07631011+01
R(3)=  5.13736815+01
R(4)=  5.19575491+01

DX=     2.540000-03

DY=     0.000000

DZ=     2.540000-03

XC= -6.15845270+01YC=  0.00000000

RADII OF CIRC. FRINGES

R(1)=  6.18269557+01
R(2)=  6.23149385+01
R(3)=  6.27971611+01
R(4)=  6.32757072+01

DX=     5.080000-04

DY=     0.000000

DZ=     5.080000-03

XC= -8.93270755+00YC=  0.00000000

RADII OF CIRC. FRINGES

R(1)=  9.74044204+00
R(2)=  1.11822230+01
R(3)=  1.24582508+01
R(4)=  1.36152087+01

DX=     1.016000-03

DY=     0.000000

DZ=     5.080000-03

XC= -1.47629096+01YC=  0.00000000

RADII OF CIRC. FRINGES

```
R(1)=  1.52845465+01
R(2)=  1.62414057+01
R(3)=  1.71449456+01
R(4)=  1.80031958+01

DX=      1.524000-03

DY=      0.000000

DZ=      5.080000-03

XC= -2.06331117+01YC=  0.00000000

RADII OF CIRC. FRINGES

R(1)=  2.09954338+01
R(2)=  2.17019386+01
R(3)=  2.23861573+01
R(4)=  2.30500746+01

DX=      2.032000-03

DY=      0.000000

DZ=      5.080000-03

XC= -2.64833140+01YC=  0.00000000

RADII OF CIRC. FRINGES

R(1)=  2.67665625+01
R(2)=  2.73242521+01
R(3)=  2.78707650+01
R(4)=  2.84068048+01

DX=      2.540000-03

DY=      0.000000

DZ=      5.080000-03

XC= -3.23335161+01YC=  0.00000000

RADII OF CIRC. FRINGES

R(1)=  3.25659208+01
R(2)=  3.30258245+01
R(3)=  3.34794116+01
R(4)=  3.39269347+01

H          4.500000+01

THETA H          7.500000+01

S          6.650000+01

THETA S          6.000000+01

DX=      5.080000-04

DY=      0.000000

DZ=      2.540000-03

XC= -1.24962114+01YC=  0.00000000

RADII OF CIRC. FRINGES

R(1)=  1.35968067+01
R(2)=  1.55505464+01
R(3)=  1.72895622+01
R(4)=  1.88689806+01

DX=      1.016000-03

DY=      0.000000

DZ=      2.540000-03
```

```
XC= -2.35716958+01YC=  0.00000000

RADII OF CIRC. FRINGES

R(1)=  2.41698070+01
R(2)=  2.53236652+01
R(3)=  2.64272301+01
R(4)=  2.74665653+01

DX=     1.524000-03

DY=     0.000000

DZ=     2.540000-03

XC= -3.46471801+01YC=  0.00000000

RADII OF CIRC. FRINGES

R(1)=  3.50568366+01
R(2)=  3.56621144+01
R(3)=  3.66497025+01
R(4)=  3.74207187+01

DX=     2.032000-03

DY=     0.000000

DZ=     2.540000-03

XC= -4.57226644+01YC=  0.00000000

RADII OF CIRC. FRINGES

R(1)=  4.60338650+01
R(2)=  4.66500397+01
R(3)=  4.72581306+01
R(4)=  4.78585949+01

DX=     2.540000-03

DY=     0.000000

DZ=     2.540000-03

XC= -5.67981486+01YC=  0.00000000

RADII OF CIRC. FRINGES

R(1)=  5.70489645+01
R(2)=  5.75473160+01
R(3)=  5.80413926+01
R(4)=  5.85312967+01

DX=     5.080000-04

DY=     0.000000

DZ=     5.080000-03

XC= -6.95846921+00YC=  0.00000000

RADII OF CIRC. FRINGES

R(1)=  7.91618541+00
R(2)=  9.55261195+00
R(3)=  1.09456443+01
R(4)=  1.21603883+01

DX=     1.016000-03

DY=     0.000000

DZ=     5.080000-03

XC= -1.24962114+01YC=  0.00000000

RADII OF CIRC. FRINGES

R(1)=  1.30549660+01
R(2)=  1.41062891+01
```

```
R(3)=  1.50844907+01
R(4)=  1.60030267+01


DX=      1.524000-03

DY=      0.000000

DZ=      5.080000-03


XC= -1.80339534+01YC=  0.00000000

RADII OF CIRC. FRINGES


R(1)=  1.84255456+01
R(2)=  1.91847744+01
R(3)=  1.99150774+01
R(4)=  2.06195307+01


DX=      2.032000-03

DY=      0.000000

DZ=      5.080000-03


XC= -2.35716958+01YC=  0.00000000

RADII OF CIRC. FRINGES


R(1)=  2.38726244+01
R(2)=  2.44633791+01
R(3)=  2.50402007+01
R(4)=  2.56040308+01


DX=      2.540000-03

DY=      0.000000

DZ=      5.080000-03


XC= -2.91094379+01YC=  0.00000000


RADII OF CIRC. FRINGES


R(1)=  2.93536491+01
R(2)=  2.98560765+01
R(3)=  3.03108263+01
R(4)=  3.07762540+01


H              4.500000+01

THETA H                 7.500000+01


S              6.650000+01

THETA S                 7.500000+01


DX=      5.080000-04

DY=      0.000000

DZ=      2.540000-03


XC= -8.13288331+00YC=  0.00000000

RADII OF CIRC. FRINGES


R(1)=  9.63353987+00
R(2)=  1.22075899+01
R(3)=  1.42926399+01
R(4)=  1.61100547+01


DX=      1.016000-03

DY=      0.000000

DZ=      2.540000-03


XC= -1.68465860+01YC=  0.00000000
```

```
RADII OF CIRC. FRINGES

R(1)=  1.95677392+01
R(2)=  2.09320502+01
R(3)=  2.22127223+01
R(4)=  2.34234784+01


DX=     1.524000-03

DY=     0.000000

DZ=     2.540000-03


XC= -2.95642927+01YC=  0.00000000

RADII OF CIRC. FRINGES

R(1)=  3.00278959+01
R(2)=  3.09342666+01
R(3)=  3.18148260+01
R(4)=  3.26716669+01


DX=     2.032000-03

DY=     0.000000

DZ=     2.540000-03


XC= -4.02799973+01YC=  0.00000000

RADII OF CIRC. FRINGES

R(1)=  4.06214881+01
R(2)=  4.12960000+01
R(3)=  4.19596701+01
R(4)=  4.26130052+01


DX=     2.540000-03

DY=     0.000000
```

```
DZ=     2.540000-03


XC= -5.09957018+01YC=  0.00000000

RADII OF CIRC. FRINGES

R(1)=  5.12658629+01
R(2)=  5.18019595+01
R(3)=  5.23325648+01
R(4)=  5.28578429+01


DX=     5.080000-04

DY=     0.000000

DZ=     5.080000-03


XC= -2.77503106+00YC=  0.00000000

RADII OF CIRC. FRINGES

R(1)=  4.63835895+00
R(2)=  7.01610180+00
R(3)=  8.76177382+00
R(4)=  1.02174278+01


DX=     1.016000-03

DY=     0.000000

DZ=     5.080000-03


XC= -8.13286331+00YC=  0.00000000

RADII OF CIRC. FRINGES

R(1)=  6.94188833+00
R(2)=  1.03722957+01
R(3)=  1.16280553+01
R(4)=  1.27608317+01
```

```
DX=     1.524000-03

DY=     0.000000

DZ=     5.080000-03


XC= -1.34907357+01YC=   0.00000000

RADII OF CIRC. FRINGES


R(1)=  1.39933385+01
R(2)=  1.49479321+01
R(3)=  1.58451198+01
R(4)=  1.66941600+01


DX=     2.032000-03

DY=     0.000000

DZ=     5.080000-03


XC= -1.88485880+01YC=   0.00000000

RADII OF CIRC. FRINGES


R(1)=  1.92115288+01
R(2)=  1.99175801+01
R(3)=  2.05994451+01
R(4)=  2.12594519+01


DX=     2.540000-03

DY=     0.000000

DZ=     5.080000-03


XC= -2.42064402+01YC=   0.00000000

RADII OF CIRC. FRINGES

R(1)=  2.44901066+01
R(2)=  2.50478039+01
R(3)=  2.55933511+01
R(4)=  2.61275101+01


DFIN
```

| | | | | |
|---|---|---|---|---|
| ...5/FOR-22 | 1 | 007742 010365 | 2 | 043252 043456 |
| ...S/FOR08 | 1 | 010366 010412 | 2 | 043457 043466 |
| ...5/FOR09 | 1 | 010413 010453 | 2 | 043467 043500 |
| ...5/FOR09 | 1 | 010454 010606 | 2 | 043501 043522 |
| ...S/FOR00 | 1 | 010607 010647 | | |
| ...S/FOR-22 | 1 | 010650 011026 | 2 | 043523 043641 |
| ...S/FOR-22 | 1 | 011027 011066 | 2 | 043642 043642 |
| ...S/FOR-22A | 1 | 011067 011131 | 2 | 043643 043662 |
| ...COMMON (COMMON BLOCK) | | | | |
| .. | 1 | 011132 011660 | 0 | 043663 044471 |
| | | | 2 | BLANK$COMMON |

...LEVEL 78-6
...: 1.757 SECONDS, 031 BLOCKS

ALL DIST. IN CM. ,ALL ANGLES IN DEGREES

H 4.500000+01

THETA H 7.500000+01

S 6.650000+01

THETA S 1.500000+01

DX= 0.000000

DY= 0.000000

DZ= 1.270000-03

XC= 3.35399976+00YC= 0.00000000

RADII OF CIRC. FRINGES

R(1)= 9.11651250+00
R(2)= 1.50551058+01
R(3)= 1.92356422+01
R(4)= 2.26608512+01

ORIGINAL PAGE IS POOR
OF POOR QUALITY

DX= 0.000000

DY= 0.000000

DZ= 2.540000-03

XC= 3.35399973+00YC= 0.00000000

RADII OF CIRC. FRINGES

R(1)= 6.80479247+00
R(2)= 1.09630958+01
R(3)= 1.30068557+01
R(4)= 1.51932019+01

DX= 0.000000

DY= 0.000000

DZ= 3.810000-03

XC= 3.35399973+00YC= 0.00000000

RADII OF CIRC. FRINGES

R(1)= 5.90615675+00
R(2)= 9.11051238+00
R(3)= 1.14333645+01
R(4)= 1.35657347+01

DX= 0.000000

DY= 0.000000

DZ= 5.080000-03

XC= 3.35399973+00YC= 0.00000000

RADII OF CIRC. FRINGES

R(1)= 5.40253133+00
R(2)= 8.00618905+00
R(3)= 1.00408636+01
R(4)= 1.10958170+01

DX= 0.000000

DY= 0.000000

DZ= 6.350000-03

XC= 3.35399973+00YC= 0.00000000

RADII OF CIRC. FRINGES

R(1)= 5.05961847+00
R(2)= 7.30839327+00
R(3)= 9.11051250+00
R(4)= 1.05089304+01

DX= 5.080000-04

DY= 0.000000

DZ= 0.000000

VERTICAL FRINGE SPACING IS 2.57819289+00

DX= 1.016000-03

DY= 0.000000

DZ= 0.000000

VERTICAL FRINGE SPACING IS 1.28909644+00

DX= 1.524000-03

DY= 0.000000

```
DZ=     0.000000

VERTICAL FRINGE SPACING IS  8.59397635-01

DX=     2.032000-03
DY=     0.000000
DZ=     0.000000

VERTICAL FRINGE SPACING IS  6.44548222-01

DX=     2.540000-03
DY=     0.000000
DZ=     0.000000

VERTICAL FRINGE SPACING IS  5.15638582-01

H          4.500000+01
THETA H            7.500000+01

S          6.650000+01
THETA S            3.000000+01

DX=     0.000000
DY=     0.000000
DZ=     1.270000-03

XC= -1.62001377+00YC=  0.00000000

RADII OF CIRC. FRINGES

R(1)=  6.23071602+00
R(2)=  1.40707239+01
R(3)=  1.81170057+01
R(4)=  2.14118276+01

DX=     0.000000
DY=     0.000000
DZ=     2.540000-03

XC= -1.62001377+00YC=  0.00000000

RADII OF CIRC. FRINGES

R(1)=  5.03165934+00
R(2)=  1.03152313+01
R(3)=  1.26017703+01
R(4)=  1.51837217+01

DX=     0.000000
DY=     0.000000
DZ=     3.810000-03

XC= -1.62001376+00YC=  0.00000000

RADII OF CIRC. FRINGES

R(1)=  4.93206690+00
R(2)=  6.23071602+00
R(3)=  1.05431607+01
R(4)=  1.24326608+01

DX=     0.000000
DY=     0.000000
```

```
DZ=     5.080000-03

XC= -1.62001377+00YC=  0.00000000

RADII OF CIRC. FRINGES

R(1)=  4.34793210+00
R(2)=  7.17388678+00
R(3)=  9.16650355+00
R(4)=  1.07974498+01

DX=     0.000000

DY=     0.000000

DZ=     6.350000-03

XC= -1.62001376+00YC=  0.00000000

RADII OF CIRC. FRINGES

R(1)=  3.95581344+00
R(2)=  6.45729119+00
R(3)=  8.23071790+00
R(4)=  9.66436985+00

DX=     5.080000-04

DY=     0.000000

DZ=     0.000000

VERTICAL FRINGE SPACING IS  2.57819289+00

DX=     1.016000-03

DY=     0.000000

DZ=     0.000000

VERTICAL FRINGE SPACING IS  1.28909644+00

DX=     1.524000-03

DY=     0.000000

DZ=     0.000000

VERTICAL FRINGE SPACING IS  8.59397635-01

DX=     2.032000-03

DY=     0.000000

DZ=     0.000000

VERTICAL FRINGE SPACING IS  6.44548222-01

DX=     2.540000-03

DY=     0.000000

DZ=     0.000000

VERTICAL FRINGE SPACING IS  5.15638582-01

H            4.500000+01

THETA H            7.500000+01

S            6.650000+01

THETA S            4.500000+01

DX=     0.000000
```

DY= 0.000000

DZ= 1.270000-03

XC= -3.06250538+00YC= 0.00000000

RADII OF CIRC. FRINGES

R(1)= 8.35665226+00
R(2)= 1.36020734+01
R(3)= 1.76397512+01
R(4)= 2.07803853+01

DX= 0.000000

DY= 0.000000

DZ= 2.540000-03

XC= -3.06250538+00YC= 0.00000000

RADII OF CIRC. FRINGES

R(1)= 6.29523297+00
R(2)= 9.99997875+00
R(3)= 1.26622009+01
R(4)= 1.46547343+01

DX= 0.000000

DY= 0.000000

DZ= 3.810000-03

XC= -3.06250538+00YC= 0.00000000

RADII OF CIRC. FRINGES

R(1)= 5.44173121+00
R(2)= [illegible].36065225+00

R( = 1.04997024+01
R(4)= 1.22567125+01

DX= 0.000000

DY= 0.000000

DZ= 5.080000-03

XC= -3.06250538+00YC= 0.00000000

RADII OF CIRC. FRINGES

R(1)= 4.95830560+00
R(2)= 7.39937073+00
R(3)= 9.21501958+00
R(4)= 1.07276504+01

DX= 0.000000

DY= 0.000000

DZ= 6.350000-03

XC= -3.06250540+00YC= 0.00000000

RADII OF CIRC. FRINGES

R(1)= 4.64415753+00
R(2)= 6.76024544+00
R(3)= 8.35665214+00
R(4)= 9.69362450+00

DX= 5.080000-04

DY= 0.000000

DZ= 0.000000

VERTICAL FRINGE SPACING IS 2.57919289+00

DX= 1.016000-03

DY= 0.000000

DZ= 0.000000

VERTICAL FRINGE SPACING IS 1.28909644+00

DX= 1.524000-03

DY= 0.000000

DZ= 0.000000

VERTICAL FRINGE SPACING IS 8.59397635-01

DX= 2.032000-03

DY= 0.000000

DZ= 0.000000

VERTICAL FRINGE SPACING IS 6.44548222-01

DX= 2.540000-03

DY= 0.000000

DZ= 0.000000

VERTICAL FRINGE SPACING IS 5.15638582-01

R 4.500000+01

THETA R 7.500000+01

S 6.650000+01

THETA S 6.000000+01

DX= 0.000000

DY= 0.000000

DZ= 1.270000-03

XC= -1.42072706+00YC= 0.00000000

RADII OF CIRC. FRINGES

R(1)= 7.65946904+00
R(2)= 1.31061258+01
R(3)= 1.69577653+01
R(4)= 2.00445058+01

DX= 0.000000

DY= 0.000000

DZ= 2.540000-03

XC= -1.42072706+00YC= 0.00000000

RADII OF CIRC. FRINGES

R(1)= 5.42930367+00
R(2)= 9.30390233+00
R(3)= 1.20329604+01
R(4)= 1.42092095+01

DX= 0.000000

DY= 0.000000

DZ= 3.810000-03

XC= -1.42072706+00YC= 0.00000000

RADII OF CIRC. FRINGES

R(1)= 4.58356785+00
R(2)= 7.68946904+00
R(3)= 9.65905230+00
R(4)= 1.16347505+01

DX= 0.000000

DY= 0.000000

DZ= 5.080000-03

XC= -1.42072706+00YC= 0.00000000

RADII OF CIRC. FRINGES

R(1)= 4.03630968+00
R(2)= 6.69715653+00
R(3)= 8.56750930+00
R(4)= 1.00975261+01

DX= 0.000000

DY= 0.000000

DZ= 6.350000-03

XC= -1.42072706+00YC= 0.00000000

RADII OF CIRC. FRINGES

R(1)= 3.66610953+00
R(2)= 6.02363241+00
R(3)= 7.68946910+00
R(4)= 9.65502369+00

DX= 1.960000-04

DY= 0.000000

DZ= 0.000000

VERTICAL FRINGE SPACING IS 2.57819289+00

DX= 1.016000-03

DY= 0.000000

DZ= 0.000000

VERTICAL FRINGE SPACING IS 1.28909644+00

DX= 1.524000-03

DY= 0.000000

DZ= 0.000000

VERTICAL FRINGE SPACING IS 8.59397635-01

DX= 2.032000-03

DY= 0.000000

DZ= 0.000000

VERTICAL FRINGE SPACING IS 6.44548222-01

DX= 2.540000-03

DY= 0.000000

DZ= 0.000000

VERTICAL FRINGE SPACING IS 5.15638582-01

```
R          4.500000+01
THETA R          7.500000+01

S          6.650000+01
THETA S          7.500000+01

DX=     0.000000
DY=     0.000000
DZ=     1.270000-03

XC=  2.56282125+00YC=  0.00000000

RADII OF CIRC. FRINGES

R(1)=  7.80926115+00
R(2)=  1.31314082+01
R(3)=  1.65208945+01
R(4)=  1.92356020+01

DX=     0.000000
DY=     0.000000
DZ=     2.540000-03

XC=  2.56282125+00YC=  0.00000000

RADII OF CIRC. FRINGES

R(1)=  5.85615950+00
R(2)=  9.46321423+00
R(3)=  1.26335667+01
R(4)=  1.49142934+01

DX=     0.000000
DY=     0.000000
DZ=     3.810000-03

XC=  2.56282125+00YC=  0.00000000

RADII OF CIRC. FRINGES

R(1)=  5.00859879+00
R(2)=  7.80926109+00
R(3)=  9.95788075+00
R(4)=  1.10446416+01

DX=     0.000000
DY=     0.000000
DZ=     5.080000-03

XC=  2.56282125+00YC=  0.00000000

RADII OF CIRC. FRINGES

R(1)=  4.52598518+00
R(2)=  6.93625945+00
R(3)=  8.70280695+00
R(4)=  1.01669071+01

DX=     0.000000
DY=     0.000000
DZ=     6.350000-03

XC=  2.56282122+00YC=  0.00000000

RADII OF CIRC. FRINGES
```

R(1)= 4.20972997+00
R(2)= 6.31059021+00
R(3)= 7.86926115+00
R(4)= 9.16662395+00

DX= 5.080000-04

DY= 0.000000

DZ= 0.000000

VERTICAL FRINGE SPACING IS 2.57819289+00

DX= 1.016000-03

DY= 0.000000

DZ= 0.000000

VERTICAL FRINGE SPACING IS 1.28909644+00

DX= 1.524000-03

DY= 0.000000

DZ= 0.000000

VERTICAL FRINGE SPACING IS 8.59397635-01

DX= 2.032000-03

DY= 0.000000

DZ= 0.000000

VERTICAL FRINGE SPACING IS 6.44548222-01

DX= 2.540000-03

DY= 0.000000

DZ= 0.000000

VERTICAL FRINGE SPACING IS 5.15638582-01

References

1. D. Gabor, Proc. Roy. Soc. (London) A197, 454 (1947).

2. F. Leith and J. Upatnieks, J. Opt. Soc. Am. 54, 1295 (1964).

3. M. H. Horman, Appl. Opt. 4, 333 (1965).

4. R. L. Powell and K. A. Stetson, J. Opt. Soc. Am. 55, 1593 (1965).

5. K. A. Haines and B. P. Hildebrand, Appl. Opt. 5, 595 (1966).

6. Jon E. Sollid, Appl. Opt. 8, 1587 (1969).

7. R. L. Kurtz, et al., Appl. Opt., 9, No. 5, May 1970.

8. R. J. Collier, C. B. Burkhardt, and L. H. Lin, Optical Holography, The Academic Press, New York, 1971.

9. R. L. Kurtz, et al., A Holographic System that Records Front Surface Detail of a Scene at High Velocity, NASA TR R-380, January 1972.

10. R. L. Kurtz, Hybrid Holographic System, U.S. Patent No. 3,535,014, June 1972.

11. R. L. Kurtz, et al., Appl. Opt., 11, No. 9, September 1972.

12. R. L. Kurtz, The Techniques of Holographic Particle Sizing, NASA TR R-404, March 1973.

13. R. L. Kurtz, Appl. Opt., 12, No. 4, April 1973.

14. V. F. Bellani and A. Sona, Appl. Opt., 13, 1337 (1974).

15. H. K. Liu and R. L. Kurtz, Proc. IEEE SE Conf. 1, 2F-2-1 (1975).

16. R. L. Kurtz, Optical Holography Applications for the Zero-g Atmospheric Cloud Physics Laboratory, NASA TR T-424, May 1974.

17. R. L. Kurtz and H. K. Liu, Holographic Nondestructive Tests Performed on Composite Samples of Ceramic-Epoxy-Fiberglass Sandwich Structure, NASA TR T-430, June 1974.

18. H. K. Liu and R. L. Kurtz, Thermal Loading in the Laser Holography Nondestructive Testing of a Composite Structure, NASA TR R-439, May 1975.

19. H. K. Liu, L. W. White, and E. R. Comeens, Quantitative Evaluation of the Holographic Interference Fringes in the Composite Mobile HNDT System, University of Alabama, College of Engineering, BER Report No. 192-74, June 1975.

20. R. L. Kurtz, Multiple patents on holography, MFS Case Nos. 21704, 20074, 20596, 21087, 22517, 22537, and 22434, Office of Patent Counsel (A&PS-PAT) Marshall Space Flight Center, Huntsville, Alabama.

21. N. L. Hecht, J. E. Minardi, D. Lewis, and R. L. Fusek, Appl. Opt. 12, 2665 (1973).

22. See Appendix B.

23. See Appendix C.

END
DATE
Filmed
8/19/76